Molecular Neurobiology (2025) 62:4319–4337
https://doi.org/10.1007/s12035-024-04536-3

ORIGINAL ARTICLE

Connexin43 Contributes to Alzheimer's Disease by Promoting the Mitochondria-Associated Membrane-Related Autophagy Inhibition

Weiwei Yu[1] · Yunong Li[1] · Yao Li[1] · Jun Hu[1] · Jun Wu[1] · Xuhui Chen[1] · Yining Huang[2] · Xin Shi[1]

Received: 16 July 2023 / Accepted: 5 October 2024 / Published online: 23 October 2024

Abstract

The perturbed structure and function of mitochondria-associated membranes (MAM), instead of the amyloid cascade, have been gradually proposed to play a basic role in the pathogenesis of Alzheimer's disease (AD). Notably, autophagy inhibition is one of the main mechanisms of MAM dysfunction and plays an important role in neuronal injury. However, the upstream molecular mechanism underlying the MAM dysfunctions remains elusive. Here, we defined an unexpected and critical role of connexin43 (Cx43) in regulating the MAM structure. The expression levels of Cx43 and mitofusin-2 (MFN2, the MAM biomarker) increase significantly in 9-month-old $APP_{swe}/PS1_{dE9}$ double-transgenic AD model mice, and there is an obvious colocalization relationship. Moreover, both AD mice and cells lacking Cx43 exhibit an evident reduction in the MAM contact sites, which subsequently promotes the conversion from microtubule-associated protein 1 light-chain 3B I (LC3B-I) to LC3B-II via inhibition mTOR-dependent pathway and then initiates the generation of autophagosomes. Autophagosome formation ultimately promotes β-amyloid (Aβ) clearance and attenuates Aβ-associated pathological changes in AD, mainly including astrogliosis and neuronal apoptosis. Our findings not only reveal a previously unrecognized effect of Cx43 on MAM upregulation but also highlight the major player of MAM-induced autophagy inhibition in Cx43-facilitated AD pathogenesis, providing a novel insight into the alternative therapeutic strategies for the early treatment of AD.

Keywords Connexin43 · Mitochondria-associated membranes · Alzheimer's disease · Autophagy · β-Amyloid

Introduction

Dementia is a general term for a class of slowly progressive degenerative diseases that are characterized by cognitive impairment, among which Alzheimer's disease (AD) is the most common form [1]. World Alzheimer Report 2014 reveals that the number of people living with dementia worldwide is estimated at 44 million with AD accounting for about 50–75% [2]. What is even more remarkable is that this number will set to almost double by 2030 and more than triple by 2050 owing to the sharp increase in the over-65 population [3]. However, the pathophysiological mechanisms underlying AD are still not well understood despite great efforts since the first case in 1907 [4], which seriously hinders the development of curative treatments for AD. Based on the two cardinal positive histopathological hallmarks in AD patients' brain, the extracellular accumulation of neuritic plaques mainly containing β-amyloid (Aβ) and intracellular neurofibrillary tangles (NFTs) mostly consisting of hyperphosphorylated tau protein, Hardy and Higgins first proposed the amyloid cascade hypothesis in 1992 [5]. The amyloid cascade hypothesis is the most prevalent hypothesis for AD pathogenesis, and both Aβ and P-tau are considered to be the targets for AD potential treatments. Unfortunately, early successes in comparative studies about the targeted therapies toward Aβ ended in the failure of clinical transformation [6]. Therefore, scholars claim that Aβ may not be

Weiwei Yu and Yunong Li are co-first authors who equally contributed to this work.

✉ Yining Huang
ynhuang@bjmu.edu.cn

✉ Xin Shi
416068846@qq.com

[1] Present Address: Department of Neurology, Peking University Shenzhen Hospital, Futian District, 1120 Lianhua Road, Shenzhen 518036, China

[2] Department of Neurology, Peking University First Hospital, 8 Xishiku Street Xicheng District, Beijing 100034, China

the primary cause of AD pathogenesis. Firstly, although the amyloid cascade hypothesis is indeed persuasive to explain how mutations in amyloid precursor protein (*APP*) and presenilin1/2 (*PS1/2*) genes contribute to family AD [7], it hardly explains the pathological changes in sporadic AD and some morphological and biochemical features in the early onset AD, mainly including aberrant calcium homeostasis [8], altered phospholipid metabolism [9], elevated serum cholesterol [10], mitochondrial dysfunction [11], and autophagy. Therefore, AD is a complex multifactorial disease, and clarifying the novel molecular mechanisms of AD is particularly important for the early intervention of AD.

Mitochondria-associated membranes (MAM) refer to the physical interaction between the endoplasmic reticulum (ER) and mitochondria, with a stable membrane distance of 10–30 nm [12]. The closely apposed membrane proves that MAM is not the simple membrane fusion but the utilization of proteinaceous tethers. Poston et al. reveal 1212 highconfidence proteins presenting at MAM in the brain, and the commonly studied MAM proteins are mitofusin2 (MFN2) and acetyl-Coenzyme A acetyltransferase 1 (ACAT1) [13]. MFN2, an outer mitochondrial membrane (OMM) profusion protein, is recognized as the first protein to participate in directly regulating the ER-mitochondria apposition through transorganellar homotypic and heterotypic interactions [14]. ACAT1, the only known enzyme for esterifying free cholesterol to cholesteryl ester, is enriched in MAM and recognized as a marker to evaluate MAM functions [15]. On the whole, MAM proteins can facilitate the two organelles to communicate with each other, both physically and biochemically, which ensures MAM to be normally involved in multiple biological processes, such as Ca^{2+} homeostasis, glucose, phospholipids, and cholesterol metabolism [16]. Emerging evidence indicates that perturbed MAM functions play a critical role in degenerative diseases, especially in the early AD cascade events. In postmortem AD brains, the contact sites between ER and mitochondria significantly increase [17], and the MAM proteins involved in Aβ generation, mainly including PS1/2 and γ-secretase, are also obviously upregulated even in $APP_{Swe/Lon}$ mice as young as 2 months [18]. Thus, MAM may play a vital role in the early AD cascade events via providing an accurate explanation for the early morphological and biochemical changes in AD. However, the upstream molecular mechanism leading to the upregulation of MAM in AD has not yet been identified. Connexin43 (Cx43), the most abundantly expressed connexin in the brain, can constitute the high-conductance membrane channel named gap junction (GJ), which guarantees more efficient intercellular communication both electrically and biochemically [19]. Cx43 is also highly expressed in the ER and mitochondria membrane [20, 21] and has the similar functions to MAM including Ca^{2+} homeostasis, oxidative stress, inflammation, lipid metabolism, apoptosis, and autophagy [16, 22], mainly through interacting with multiple proteins presenting in MAM [23–26]. Furthermore, Cx43 and MAM play a synchronous regulatory role in AD pathogenesis [27]. Studies have shown that Cx43 activity is significantly increased in the postmortem AD brains and AD model mice [28], which subsequently reduces the effective clearance of abnormally aggregated proteins and damage/dead cells by negatively regulating autophagy [29], ultimately promoting Aβ deposition and leading to AD. Despite many similarities between Cx43 and MAM, no studies have been conducted on the correlation between Cx43 and MAM in AD.

Based on the current available researches, we speculate whether Cx43 and MAM are on the same regulatory pathway and that Cx43 is even the upstream regulator of MAM. Interestingly, our study has revealed an obvious immunostaining colocalization between Cx43 and MFN2 in brains of the double-transgenic $APP_{swe}/PS1_{dE9}$ mice (APP/PS1 mice for short), which preliminarily confirms our speculation and encourages us to further address the role of Cx43 in MAM structure and function. Subsequently, we utilize Cx43 knockout or siRNA inhibition in AD mice and cells to demonstrate that Cx43 deficiency not only reduces the contact sites between the ER and mitochondria but also eliminates the MAM-induced autophagy inhibition by restraining mechanistic target of rapamycin (mTOR)-dependent signaling pathway. Activated autophagy thereby promotes the clearance of abnormal Aβ aggregation in AD and decreases the subsequent neuronal toxicity, finally attenuating Aβ-associated pathological changes in AD. These expected findings will indeed provide a theoretical basis for early intervention of AD and help to discover the new clinical treatment strategies and potential biological intervention targets.

Materials and Methods

Animals

The double-transgenic APP/PS1 mice were obtained from Nanjing Biomedical Research Institute of Nanjing University (China) as an AD model, and the globally heterozygous Cx43 ($Cx43^{\pm}$) mice were acquired from Shanghai Biomodel Organism Science & Technology Co. (China). Then, APP/PS1$Cx43^{\pm}$ mice were generated by crossbreeding APP/PS1 mice with $Cx43^{\pm}$ mice, and wild-type (WT) mice routinely served as controls. Mouse genotypes were identified via PCR technology. Mice used in our experiment were housed in the specific pathogen-free (SPF) animal facility of Peking University First Hospital with a 12-h light/dark cycle and free access to food and water. All experiments on mice were conducted at Peking

University First Hospital and in compliance with the ethics approval obtained from Peking University First Hospital.

Immunohistochemistry

After the intraperitoneal anesthesia with 40 mg/kg sodium pentobarbital, brains were dissected from mice with phosphate buffer saline (PBS) transcardially perfused, which were fixed in 4% paraformaldehyde (PFA) for 24 h and then equilibrated in a 30% sucrose solution, ultimately embedded in paraffin. The paraffin-embedded brains were sectioned at 4 μm. After a series of dewaxing, rehydration, and antigen retrieval, brain sections were incubated with 10% normal goat serum for 1 h at room temperature (RT). Anti-myelin-associated glycoprotein (MAG) antibody was used to incubate sections overnight at 4 °C followed by the incubation of secondary antibody for 1 h at RT. Finally, the sections were treated with diaminobenzidine (DAB) to observe the MAG staining in the corpus callosum (CC) by light microscopy.

Hematoxylin–Eosin (HE) Staining

Paraffin-embedded sections were dewaxed with xylene three times for 10 min followed by rehydration through varying concentrations of ethanol from 100 to 70%. The sections were stained with hematoxylin for 1 min, and the residual hematoxylin was removed with PBS. The hematoxylin-stained sections were then treated with eosin stain for 30 s. Finally, these sections were dehydrated with 70 to 100% ethanol followed by xylene transparent. The stained sections were covered by slips and then observed with a light microscope to investigate the white matter (WM) in CC and hippocampal neurons.

Tissue Immunofluorescence Staining and Confocal Microscopy

Dissected brains as described above were embedded in O.C.T. compound and sectioned at 6 μm. The sections were fixed with 4% PFA and then rinsed with PBS to eliminate the remaining PFA. After being blocked with 10% normal goat serum, the sections were incubated with different primary antibodies. After an overnight incubation at 4 °C, the sections were rinsed with PBS and applied with the corresponding fluorochrome-labeled secondary antibodies for 1 h at RT. Finally, coverslips were used to cover sections with the fluorescent mounting medium. Fluorescence images were examined under a fluorescence microscope.

Evaluation of MAM and Myelin Sheath by Transmission *Electron* Microscopic (TEM)

The ER-mitochondrial contacts and myelin sheath were evaluated by TEM as previously described [30]. Briefly, a 1 mm^3 mass of brain tissue or cultured cells was prepared and fixed in 2.5% glutaraldehyde solution overnight at 4 °C, then rinsed in phosphate buffer. The samples were post-fixed in 2% osmic acid (OsO4) for 2 h, dehydrated in ethanol and acetone, embedded in an 812 epoxy embedding kit, and finally sectioned on a Leica EM UC6/FC6 Ultramicrotome. The sections were transferred to copper grids, counter staining of which was performed with uranyl acetate and lead acetate. The images of specimens were obtained through TEM. The fraction of mitochondria membrane in contact with ER within a range of 50 nm was measured and normalized to the mitochondria perimeter via ImageJ software.

Cell Culture and Viral Transfection

The popular *SH-SY5Y* neuroblastoma cell line was purchased from the American Type Culture Collection (ATCC; USA). *SH-SY5Y* cells were cultured in DMEM:F12 containing 10% fetal bovine serum and 100 U/mL penicillin and streptomycin and incubated in a humidified incubator (95% air/5% CO_2) at 37 °C. To simulate the characteristic pathological changes of neurons in AD, we generated the constructs designed to encode full-length human APP with both K670N/M671L (*Swedish*) and V717I (*London*) mutations (APPSL, referred to as APP) from the JTS Scientific (GenBank accession no: NM_201414). Lentivirus harboring anti-puromycin JLVO-EF1a-APuro (JLV-Puro) was recognized as a negative control (NC). Lentivirus supernatants diluted in fresh culture medium containing transfection enhancer polybrene were used to transfect *SH-SY5Y* cells cultured in 6-well plates. After 72 h transfection, cells were collected to identify the transfection efficiency via western blot analysis.

Small Interfering RNA (siRNA) Transfection

Human Cx43 siRNA and non-silencing control siRNA were obtained from JTS scientific (Beijing, China). siRNA transfection was performed as previously described [31]. *SH-SY5Y* cells were incubated in 6-well plates to 70% confluence and then transiently transfected with 20 mM siRNA that bounds to Lipofectamine™ 3000 Reagent. After the transfected cells were incubated for 24 h in a humidified incubator at 37 °C in 5% CO_2. Cells were finally collected 72 h post-transfection to identify the transfection efficiency through western blot analysis.

Enzyme-Linked Immunosorbent Assay (ELISA) Kit for Aβ42

The quantitative measurement of Aβ42 in a culture medium was performed using an Aβ42 ELISA kit (CEA946Hu) following the instructions. Briefly, aliquots of 50 μL standards or samples were added to the appropriate microplate

wells, respectively. Fifty microliters detection reagent A was immediately added to each well and then incubated together for 1 h at 37 °C. After aspirating the mixed solution and then removing any remaining wash buffer, each well was added 100 µL detection reagent B and incubated for 30 min at 37 °C. After repeating the aspiration/wash process, each well was added 90 µL substrate solution followed by 50 µL stop solution. Finally, the absorbance was measured at 450 nm on a microplate reader, and the concentrations of samples were obtained from the generated standard curve.

Flow Cytometric Analyses of Apoptosis Assays

Apoptotic *SH-SY5Y* cells were detected using an Annexin V-FITC Apoptosis Detection Kit (Beyotime, C1062M) following the manufacturer's protocol. Transfected cells were cultured in a humidified incubator at 37 °C in 5% CO_2 for 48–72 h and subsequently collected with trypsin without EDTA. The harvested cells were centrifugated and resuspended with 1 mL PBS. Approximately 5×10^6 cells were taken from each group to be incubated with 5 µL Annexin FITC and 10 µL propidium iodide (PI) without light for 15 min at RT. The stained cells were analyzed by flow cytometric, and the statistical significance was analyzed via GraphPad Prism 7.0 software.

Cellular Immunofluorescence Staining and Confocal Microscopy

Cells were fixed with 4% fresh PFA for 15 min and then washed with PBS to remove the remaining PFA. After being treated with 0.2% Triton X-100 in PBS to increase membrane permeability, cells were blocked with 10% goat serum for 1 h at RT and then incubated with different primary antibodies at 4 °C overnight. Then, the cells were treated with corresponding secondary antibodies in the dark for 1 h at RT. Finally, the mounted cells were observed under a fluorescence microscope (DMi8, Leica, Germany).

Detection of Apoptosis by Terminal Deoxynucleotidyl Transferase-Mediated dNTP Nick End Labeling (TUNEL) Staining

In situ apoptosis was detected by a one-step TUNEL apoptosis assay kit (Beyotime, C1088) according to the manufacturer's instructions. Briefly, cells were fixed by 4% PFA for 30 min and then rinsed twice with PBS to remove residual PFA. Cells were permeabilized for 5 min in PBS containing 0.3% Triton X-100. After two washes, cells were incubated with 50 µL TUNEL detection solution in the dark for 1 h at 37 °C. Then, cells were embedded in a mounting medium containing DAPI, and apoptotic nuclei were observed as green fluorescence via a fluorescent microscope (DMi8, Leica, Germany).

Western Blotting Analysis

Isolated brains or cultured cells were lysed in an SDS Lysis Buffer (Beyotime, P0013G) containing 1 mM phenylmethanesulfonyl fluoride (PMSF, Beyotime, ST506). Total protein concentrations were detected via a Pierce BCA Protein Assay Kit (Thermo Scientific™, USA). Equal extract proteins (30 mg) were subjected to gradient concentration SDS/PAGE gel electrophoresis and then transferred to PVDF membranes (MilliporeSigma). After blocked with 5% nonfat milk solution for 1 h at RT, the PVDF membranes were incubated with the primary antibodies at 4 °C overnight. Subsequently, the membranes were incubated with goat anti-mouse or rabbit horseradish peroxidase (HRP)-conjugated secondary antibodies for 1 h at RT. Protein bands were visualized using an enhanced chemiluminescence system.

Statistical Analysis

Values are presented as mean ± standard deviation (SD), and n corresponds to the number of independent experiments. Statistical analysis was performed on raw data with GraphPad Prism 7.0 software (GraphPad Software, Inc., La Jolla, CA, USA). Kolmogorov–Smirnov D test (K-S test) was used to assess normality, and one-way ANOVA was used to analyze the variance followed by Bonferroni post hoc tests or Student's t-tests. The threshold for significance was set at $P < 0.05$. Fluorescence quantification and colocalization analysis of immunofluorescence were performed using ImageJ.

Results

Increased Cx43 and MFN2 in APP/PS1 Mice Show an Obvious Colocalization

To further identify the exact correlation between Cx43 and Aβ, we established an AD model, the APP/PS1 mice, and raised to various months of age, up to 3, 6, 9, and 12 months old. Then, the brain sections obtained from APP/PS1 mice at different months of age (3 m, 6 m, 9 m, 12 m) were double-labeled with Cx43 and Aβ42 to observe the dynamic change of Cx43 and Aβ42 with age. The result showed that Aβ42 deposition gradually increased with the age of APP/PS1 mice, and the Cx43 immunoactivity was also synchronously enhanced around Aβ42 plaques (Fig. 1A). In line with the Cx43 and Aβ42 double immunostaining result, the expression levels of Cx43 and Aβ42 analyzed by western blot also displayed the significantly synchronous increases

with the APP/PS1 mice grew older (Fig. 1B), which further suggested that Cx43 was indeed involved in the Aβ42 formation. According to the quantitative analysis for optical densities of Aβ42 bands, Aβ42 expression already increased significantly by the time the mice were 9 months old (Fig. 1C). Therefore, the subsequent analyses of animal experiments were done with 9-month-old mice, when Aβ42 plaques were scattered enough to analyze the underlying mechanism of Cx43-induced Aβ42 formation.

The alteration in MFN2 expression is closely associated with MAM structure, the deficiency of which contributes to a lower ER connection with mitochondrial fraction [32]. Thus, to investigate whether there is a correlation between Cx43 and MAM in 9-month-old APP/PS1 mice, we performed immunostaining for Cx43 and MFN2 in brain sections. The result revealed that the fluorescence intensities of both Cx43 and MFN2 in 9-month-old APP/PS1 mice significantly increased compared with WT mice of the same

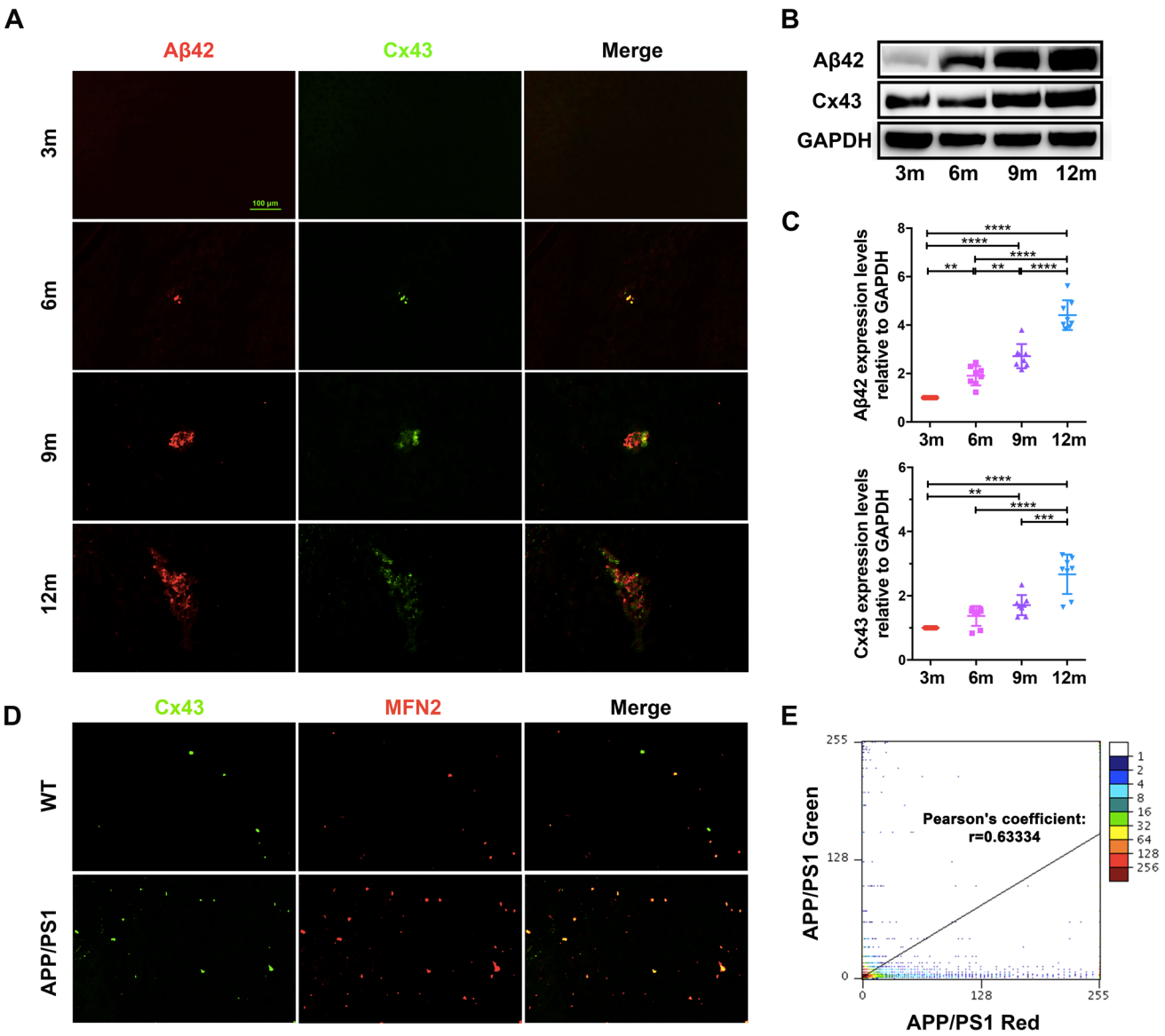

Fig. 1 Cx43 is colocalized with the MAM structural marker MFN2 in APP/PS1 mice. **A** Double immunostaining for Cx43 (green) and Aβ42 (red) in APP/PS1 mice at different months of age (3 m, 6 m, 9 m, 12 m) showing that the immunoactivity of Cx43 around Aβ42 plaques increased significantly with the increase of the age of APP/PS1 mice. Scale bar, 100 μm. **B** Western blot assay to detect the Aβ42 and Cx43 expression levels in APP/PS1 mice at different months of age (3 m, 6 m, 9 m, 12 m). **C** Quantitative analysis of protein levels relative to GAPDH. **D** Double immunostaining for Cx43 (green) and MFN2 (red) in 9-month-old WT and APP/PS1 mice showing an obvious colocalization between Cx43 and MFN2, a MAM structural marker. Scale bar, 100 μm. **E** Scatter J is used for colocalization relationship analysis, and Pearson's coefficient ($r=0.63334$) further demonstrates a colocalization relationship between Cx43 and MFN2 in 9-month-old APP/PS1 mice. $^{****}P<0.0001$, $^{***}P<0.001$, $^{**}P<0.01$ versus WT mice, $n>6$ mice for each group

age, and there also was an obvious colocalization phenomenon (Fig. 1D). The quantitative analysis of fluorescence colocalization by Scatter J showed that Pearson's coefficient ($r = 0.63334$) further proved a colocalization of Cx43 and MFN2 in 9-month-old APP/PS1 mice (Fig. 1E). These findings indicate that Cx43 may be involved in Aβ42 deposition through regulating MAM structure, since Cx43 and MFN2 display an obvious correlation.

Cx43 Is a Major Contributor to MAM Formation and Aβ42 Deposition

Prompted by the finding that there was an obvious colocalization between Cx43 and MFN2, we further examined whether Cx43 can be performed as a mediator to regulate the MAM formation by establishing a Cx43 heterozygous mouse model via CRISPR/Cas-9 gene-targeting technology to hybridize with APP/PS1 mice, generally producing four experimental groups: WT, Cx43$^{\pm}$, APP/PS1, and APP/PS1Cx43$^{\pm}$ mice. We raised mice to the age of 9 months and evaluated the ER-mitochondrial contact sites through TEM. TEM results demonstrated that there was a significant increase of the ER-mitochondrial contact sites (mark with green polygons in the enlarged images and its corresponding pattern diagrams) in APP/PS1 mice compared with WT and Cx43$^{\pm}$ mice as exhibited in Fig. 2A, and Cx43 knockout could obviously eliminate the increased MAM formation in APP/PS1 mice. The quantitative analysis result revealed that the percentage of mitochondria membrane in contact with ER in APP/PS1 mice was about twice that in the other three groups, and there were no significant differences among the other three groups (Fig. 2B). ACAT1, abundant in MAM interface, is generally regarded as the indirect measurement of MAM activity [33]. We thereby performed western blot for MFN2 and ACAT1 proteins to further evaluate the effect of Cx43 deletion on MAM structure and activity. The result revealed that the expression of MFN2 ($P < 0.0001$) and ACAT1 ($P < 0.0001$) significantly increased in APP/PS1 mice compared with WT mice, but decreased in APP/PS1Cx43$^{\pm}$ mice compared with APP/PS1 mice (Fig. 2C). The quantitative analysis of optical densities revealed a 3.5-fold of MFN2 and 1.6-fold of ACAT1 expression in APP/PS1 mice compared to APP/PS1Cx43$^{\pm}$ mice (Fig. 2D), which further suggested that Cx43 deficiency can affect the structure and activity of MAM in APP/PS1 mice. There was no difference of MFN2 and ACAT1 expression between WT and Cx43$^{\pm}$ mice.

Moreover, the role of Cx43-mediated MAM alteration in Aβ deposition was investigated through performing Aβ42 immunostaining on brain sections, which was analyzed using a fluorescent microscope. The results showed that WT and Cx43$^{\pm}$ mice only displayed trace Aβ42 fluorescent, while APP/PS1 mice exhibited substantial Aβ42 fluorescent, the latter of which can be significantly reduced by Cx43 deficiency (Fig. 2E). Similar result was obtained from the western blot analysis for evaluating the Aβ42 expression level in these four groups. The Aβ42 expression levels both in APP/PS1 and APP/PS1Cx43$^{\pm}$ mice, especially in APP/PS1 mice, were higher than that in WT and Cx43$^{\pm}$ mice (Fig. 2F). The quantification of Aβ42 bands revealed that the expression of Aβ42 increased almost 2.5-fold ($P < 0.0001$) in APP/PS1 mice compared to WT and Cx43$^{\pm}$ mice and about 1.5-fold ($P = 0.0011$) compared to APP/PS1Cx43$^{\pm}$ mice (Fig. 2G). Together, Cx43 can be suggested as a major player in the MAM formation, and Cx43-mediated MAM alteration can subsequently affect the Aβ42 generation.

Cx43-Mediated MAM Formation Aggravates Aβ-Associated Pathogenesis in APP/PS1 Mice

White matter lesions (WML) are primarily characterized by demyelination with/without axonal loss companied by the associated reactive gliosis, generally resulting in the histologically rarefaction of cerebral white matter [34]. Notably, it has been indicated that there is a much stronger association between Aβ deposition with white matter lesions (WML) in AD [35]. Therefore, we purposely explore whether Cx43-mediated MAM formation will be sufficient to contribute to the Aβ-associated pathogenesis in APP/PS1 mice in the next set of analyses, mainly including WML and neuronal injury. HE staining was first performed to evaluate the histological alterations in CC and hippocampal neurons. As demonstrated in Fig. 3A, the nerve fibers in the white matter of WT and Cx43$^{\pm}$ mice were neatly aligned and wrapped in dense myelin sheaths (the area between the two yellow dotted lines). However, the white matter in APP/PS1 mice was featured by the disarrangement of nerve fibers and reduction of myelinated fibers, which can be obviously alleviated by decreasing Cx43 expression in APP/PS1 mice (Fig. 3A indicated in the area between the two yellow dotted lines). Simultaneously, a severe loss of neurons in CA1 stratum pyramidal can also be observed in APP/PS1 mice compared to APP/PS1Cx43$^{\pm}$ mice through hippocampus HE staining, although there were also scattered apoptotic neurons in APP/PS1Cx43$^{\pm}$ mice (Fig. 3A, indicated by the white arrows). There was no significant histological difference between the WT and Cx43$^{\pm}$ mice both in white matter and neuronal loss. To investigate the ultrastructural alterations in white matter, we used TEM to observe the myelin sheath. The structure of the myelin sheath in APP/PS1 mice had the myelinated lamina separation, distortions, and reduction (Fig. 3B red arrow), and even part of the myelin sheath had obvious segmental demyelination, axon atrophy, and swelling (Fig. 3B red star). Differently, the other three group mice had more myelinated fibers with normal morphology, and the myelin sheaths were thicker and more uniform (Fig. 3B). Hence,

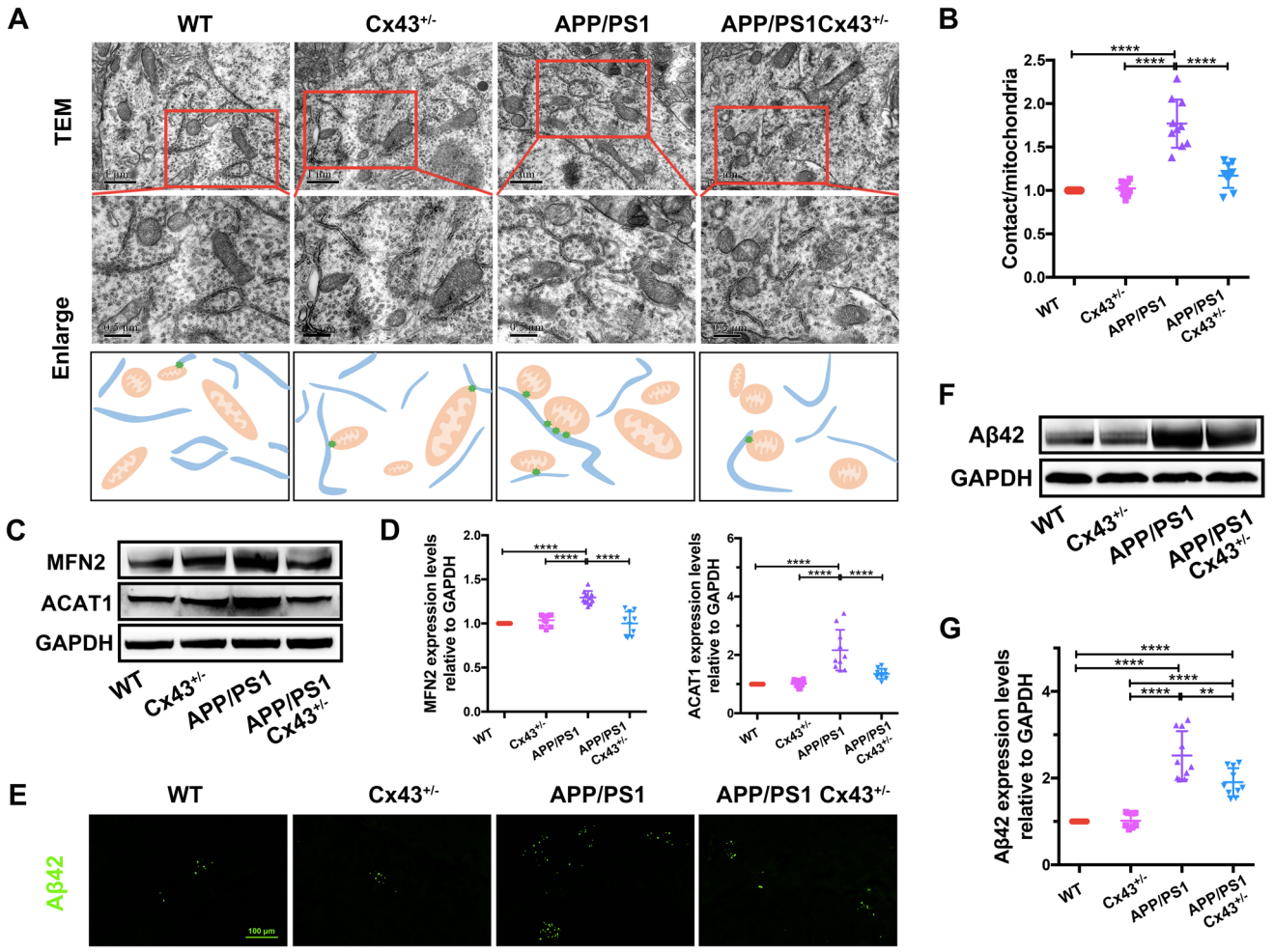

Fig. 2 Cx43-mediated MAM increase promotes Aβ deposition in APP/PS1 mice. **A** Representative TEM images of the mitochondria membranes in contact with ER in four groups of mice reveal a significant increase of mitochondrial-ER coupling (at the top) in APP/PS1 mice compared with the other three groups, which can be more clearly observed in the enlarged images and its corresponding pattern diagrams (below). Scale bars, 1 μm (at top) and 500 nm (below); green polygons mark ER-mitochondria contact sites. **B** Quantitative analysis of the percentage of mitochondria membranes in contact with ER by ImageJ. **C** Representative western blot images of MFN2 and ACAT1 were used to evaluate the MAM structure and activation. **D** Quantitative analysis of optical densities of the bands relative to GAPDH. **E** Representative immunostaining images for Aβ42 in four groups of mice showing an obvious decrease in fluorescence intensity of Aβ42 in APP/PS1Cx43± mice compared with APP/PS1 mice. Scale bar, 100 μm. **F** Representative images of Aβ42 measured by western blot in four groups of mice. **G** Quantitative analysis of optical densities of Aβ42 relative to GAPDH. $^{****}P < 0.0001$, $^{**}P < 0.01$ versus WT mice, $n > 6$ mice for each group

based on these interesting biological phenomena in white matter, which molecule is involved? Myelin-associated glycoprotein (MAG), expressed exclusively in oligodendrocytes and Schwann cells, plays the generally known pathophysiological roles in maintaining myelin integrity and inhibiting axonal regeneration [36]. We performed an immunohistochemistry staining assay with MAG to identify the myelin integrity. The results clearly revealed that the myelin integrity in CC of APP/PS1 mice was obviously compromised, mainly manifested as the reduction and attenuation of MAG staining and the obvious increase of white matter vacuoles, and this phenomenon could be alleviated in APP/PS1Cx43± mice and was not even observed in WT and Cx43± mice (Fig. 3C). Additionally, astroglia immunolabeled for glial fibrillary acidic protein (GFAP) was significantly enhanced in APP/PS1 and APP/PS1Cx43± mice compared to WT and Cx43± mice, especially in APP/PS1 mice (Fig. 3D), which indicates a more significant activation of astroglia in APP/PS1 mice than that in APP/PS1Cx43± mice. Furthermore, a western blot was thereby used to verify the WML and astrocyte activation. Consistent with the immunostaining results, the expression level of MAG in APP/PS1 mice was significantly lower than that in the other three group mice, while GFAP expression in APP/PS1 mice was obviously higher than that in APP/PS1Cx43± mice, both of which were higher than that in WT and Cx43± mice (Fig. 3E, F). These

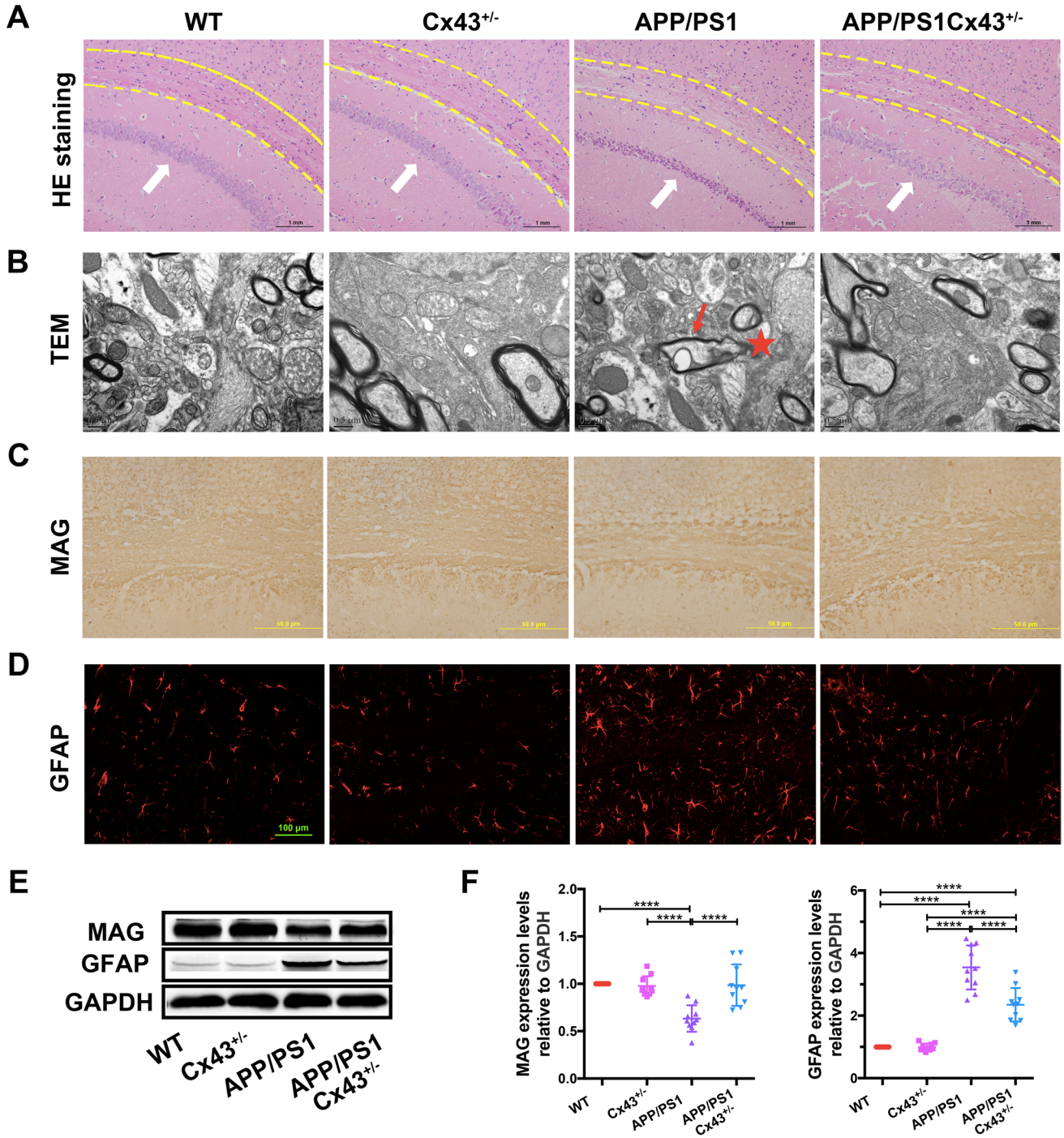

Fig. 3 Cx43-mediated MAM formation further accelerates WML and neuronal injury in APP/PS1 mice. **A** HE staining was used to investigate the pathological changes of white matter in CC (critical areas indicated between two yellow dotted lines) and hippocampal neurons (white arrows) in four groups of mice. Scale bar, 1 mm. **B** Representative TEM images for observing the ultrastructural alterations of myelin sheath of four group mice indicating a significant decrease of myelinated lamina (red arrow) and segmental demyelination (red star). Scale bar, 500 nm. **C** Representative immunostaining images for MAG showing an obvious decrease of MAG staining in APP/PS1 mice. Scale bar, 50 μm. **D** Representative images depict immunofluorescent labeling of GFAP in four groups of mice to indicate the astrogliosis exhibiting an evident activation of astroglia in APP/PS1 mice. Scale bar, 100 μm. **E** Western blot analysis for GFAP and MAG expressions with GAPDH used as an internal control. **F** Quantitative analysis of GFAP and MAG proteins relative to GAPDH. $^{****}P < 0.0001$ versus WT mice, $n > 6$ mice for each group

findings reveal that Cx43 deficiency-mediated MAM reduction may attenuate Aβ-associated pathogenesis in APP/PS1 mice, mainly including WML pathogenesis, reactive astrogliosis, and irreversible neuronal injury.

Cx43-Mediated MAM Formation Impairs Autophagy via *Activating the mTOR-Dependent Pathway*

So, by what mean does the Cx43-mediated MAM increase promote the Aβ42 deposition and Aβ42-associated pathological changes in APP/PS1 mice. Emerging evidence has demonstrated that MAM is involved in autophagy, and autophagy generally facilitates the degradation and clearance of APP and its cleavage product Aβ in AD [37, 38]. Thus, impaired autophagy will decrease Aβ clearance, and enhanced Aβ deposition in turn can even promote defective autophagy, thus contributing to neuronal toxicity and cognitive impairment [33, 39]. We set out to explore whether autophagy is involved in Aβ42 deposition due to Cx43-mediated MAM increase. The protein P62, one of the widely used autophagy markers, is itself degraded by autophagy [40], and P62 accumulation occurs when autophagy is inhibited. Microtubule-associated protein 1 light-chain 3 (LC3) is the only protein that localizes to all types of autophagic membranes among known autophagy-related gene 8 (ATG8)-encoded proteins [41]. Thus, LC3, specifically LC3B, is commonly regarded as another widely used autophagosome marker to monitor autophagy progression through the conversion from LC3 I to LC3 II [42]. Notably, P62 can directly bind to LC3 via a short LC3 interaction region serving as a mechanism of transferring the selective autophagic cargo for degradation by autophagy [43]. Here, we operated the double immunostaining and western blot for P62- and LC3B-based biochemical analysis of autophagy progression. The double immunostaining for LC3B and P62 demonstrated an obviously weak fluorescence intensity and colocalization of P62 with LC3B puncta in APP/PS1 mice compared to WT and Cx43$^{\pm}$ mice, which proved that APP/PS1 mice showed an impaired autophagy function (Fig. 4A). However, the intensified colocalization of P62 with LC3B puncta was observed in APP/PS1Cx43$^{\pm}$ mice compared to APP/PS1 mice, indicating that Cx43 knockout can rescue autophagy deficiency in APP/PS1 mice (Fig. 4A).

Meanwhile, western blot analysis for autophagy flux further confirmed that both LC3B-I and LC3B-II form in WT and Cx43$^{\pm}$ mice were higher than those in APP/PS1 and APP/PS1Cx43$^{\pm}$ mice, suggesting that LC3B-II is constitutively delivered to lysosomes for degradation under normal growth condition, but not in APP/PS1 mice (Fig. 4B). Nevertheless, the predominant form of LC3B detected was LC3B-II in APP/PS1Cx43$^{\pm}$ mice, with only a trace amount of LC3B-I detected, which was the opposite in APP/PS1 mice (Fig. 4B). The quantitative analysis revealed an approximate 2.5-fold of LC3B-II/I ration in APP/PS1Cx43$^{\pm}$ mice to APP/PS1 mice (Fig. 4C), and the significantly increased LC3B conversion (LC3B-I to LC3B-II) indicated an autophagy flux in APP/PS1Cx43$^{\pm}$ mice. Simultaneously, the P62 degradation assay revealed that the amount of P62 was obviously increased in APP/PS1 and APP/PS1Cx43$^{\pm}$ mice compared to WT and Cx43$^{\pm}$ mice, especially in APP/PS1 mice (Fig. 4B, C), which further identified a more severe autophagy inhibition in APP/PS1 mice compared to APP/PS1Cx43$^{\pm}$ mice. Our results show that autophagy could be still activated in APP/PS1Cx43$^{\pm}$ mice, although it was severely impaired in APP/PS1 mice.

mTOR, a sub-signaling protein of phosphoinositide 3-kinase (PI3K) and protein kinase B (PKB; also known as AKT), has been reported to be hyperactivated in AD, which is deeply involved in the Aβ hyperphosphorylation and aggregation by inhibiting autophagy [44, 45]. Therefore, we performed a western blot assay to investigate whether the PI3K/AKT/mTOR signaling pathway participates in the MAM-induced autophagy inhibition in APP/PS1 mice. We detected that the total mTOR and AKT expression levels did not differ among the four groups, while P-mTOR ($P < 0.0001$) and P-AKT ($P < 0.0001$) expression levels were significantly lower in APP/PS1Cx43$^{\pm}$ mice than that in the other three groups without statistical difference observed (Fig. 4D, E). Taken together, these findings indicate that autophagy function is impaired in APP/PS1 mice, and MAM reduction mediated by Cx43 deletion may attenuate autophagy impairment by inhibiting the mTOR-dependent signaling pathway.

Cx43-Deficient AD Cells Are Defective in the MAM Formation

We further identified the role of Cx43 in the MAM formation in the neural cell line *SH-SY5Y*. The *SH-SY5Y* cells were treated with lentivirus transfection as described in the "Materials and Methods" section to mimic the major AD pathological changes by increasing the Aβ expression, and the transfection efficiency in *SH-SY5Y* cells was confirmed via western blot assay. The results revealed that there was an obviously increased expression of Aβ42 in JLV-APP-treated cells (Fig. 5A), and the quantitative analysis of optical densities showed an approximate four-fold of Aβ42 in JLV-APP-treated cells compared to that in NC-treated cells (Fig. 5B), which perfectly mimics one of the characteristic pathological changes in AD. Meanwhile, the cells were also transfected with Cx43 siRNA to diminish the expression level of Cx43. Western blot results demonstrated a significant downregulation of Cx43 expression in Cx43 siRNA-treated cells (Fig. 5C, D), indicating that Cx43 was successfully reduced transiently by an siRNA-based technique. After verifying the transfection

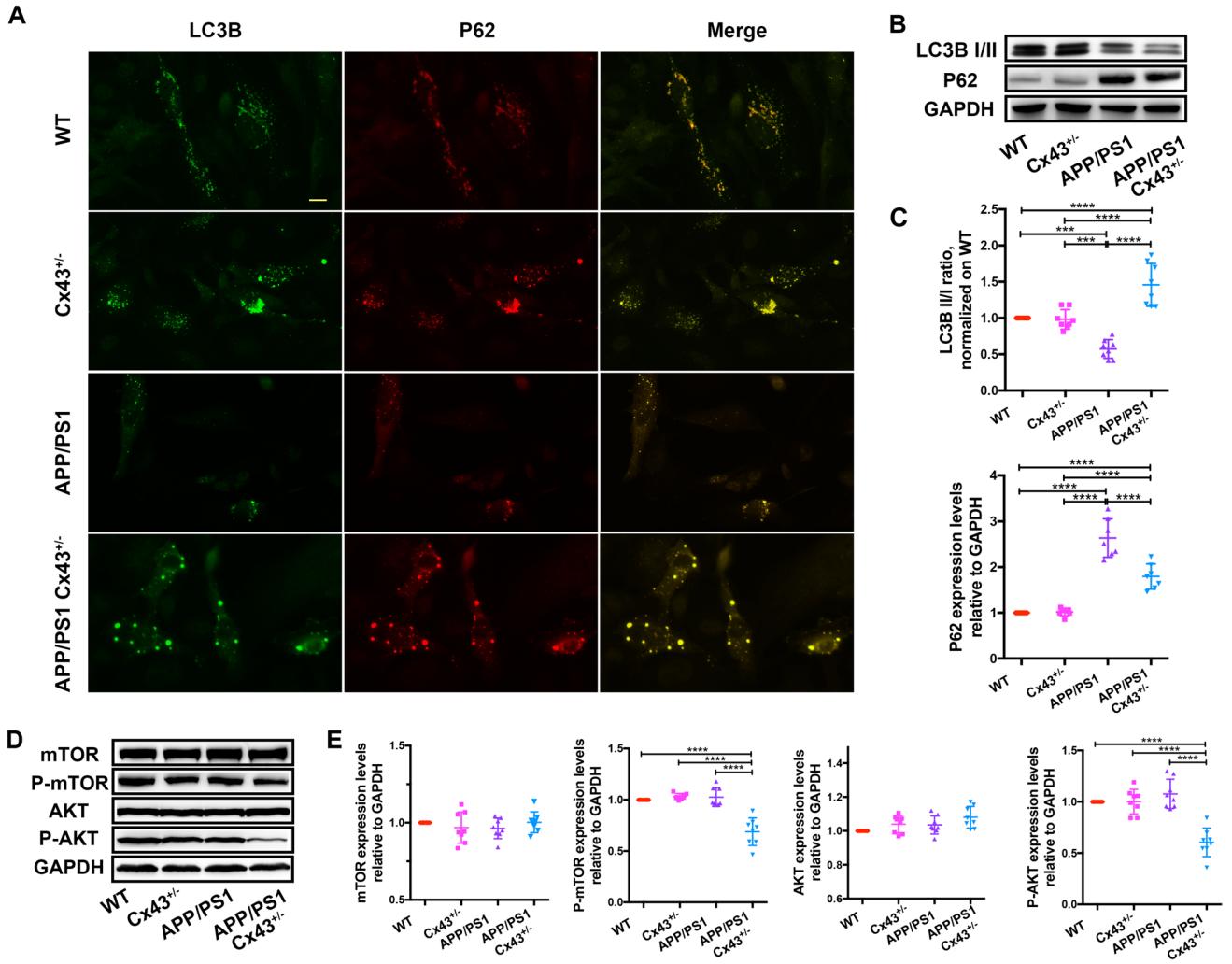

Fig. 4 Cx43-mediated MAM increase impairs autophagy by activating mTOR-dependent pathway. **A** Representative images of double immunostaining for LC3B (green) and P62 (red) in four groups of mice showing a significant autophagy deficiency in APP/PS1 mice, which can be rescued by Cx43 knockout. Scale bar, 50 μm. **B** Western blot analysis for LC3B and P62 expression with GAPDH used as an internal control to determine autophagic flux. **C** Quantitative analysis of LC3B and P62 proteins relative to GAPDH. **D** Western blot was used to evaluate the expression levels of proteins associated with the mTOR-dependent autophagy signaling pathway. **E** Quantitative analysis of optical densities of bands in Fig. 4D relative to GAPDH. $^{****}P<0.0001$, $^{***}P<0.001$ versus WT mice, $n>6$ mice for each group

efficiencies of lentivirus and siRNA, we divided the cells into four experimental groups according to the groups in vivo: NC, siRNA, JLV-APP, siRNA + JLV-APP. Then, we carried out a TEM experiment to investigate detailly the role of Cx43 in MAM formation in AD cells. Consistent with the results in vivo, the TEM results of cells showed an increase of the ER-mitochondrial contact points in JLV-APP-treated cells, which can be reduced via Cx43 siRNA treatment, and there was no difference in the ER-mitochondrial contact points between NC- and siRNA-treated cells (Fig. 5E). The quantitative analysis of TEM images also exhibited that the percentage of mitochondria membranes in contact with ER in JLV-APP-treated cells was about 1.5 times that of the siRNA + JLV-APP-treated cells (Fig. 5F). At the same time, MFN2 immunostaining demonstrated an obvious increase in fluorescence intensity of MFN2 in JLV-APP-treated cells compared with the other three groups of treated cells (Fig. 5G). Similar results were also observed in western blot analysis, where the increased expressions of both MFN2 and ATCA1 were noted in JLV-APP-treated cells compared with siRNA + JLV-APP-treated cells, while there was no significant difference in the expression of both MFN2 and ATCA1 among the other three cell groups (Fig. 5H, I). These findings further suggest that Cx43 plays an important role in the MAM formation, and Cx43 deficiency can reduce the ER-mitochondrial contact points in response to JLV-APP-induced AD alterations *in vitro*.

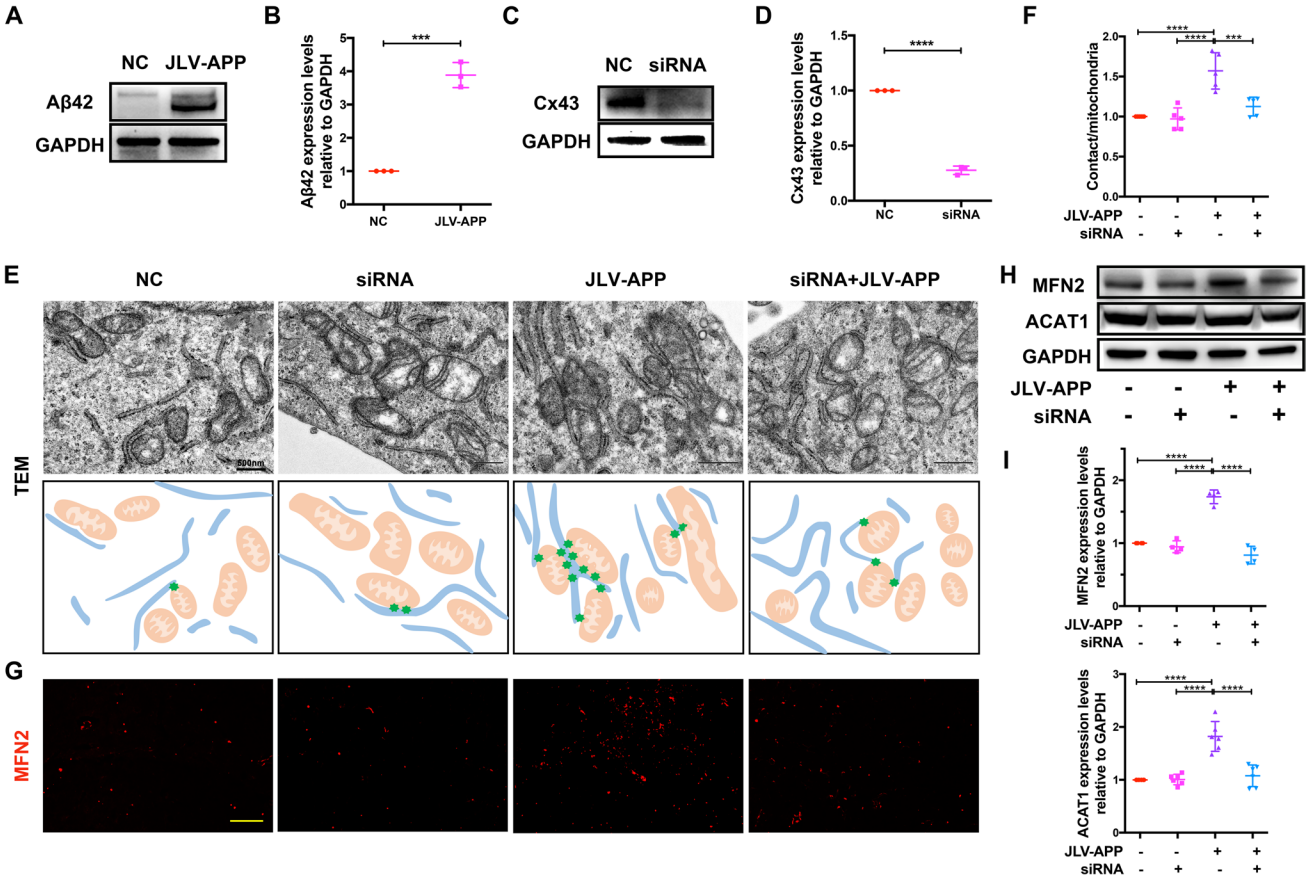

Fig. 5 Cx43 contributes to the MAM formation in AD cells. **A** Western blot analysis for Aβ42 to identify the transfection efficiency of JLV-APP. **B** Quantitative analysis of Aβ42 relative to GAPDH. **C** Western blot analysis for Cx43 to identify the transfection efficiency of Cx43 siRNA. **D** Quantitative analysis of Cx43 relative to GAPDH. **E** Representative TEM images for observing the percentage of mitochondria membrane in contact with ER in cells showing an obvious increase of mitochondrial-ER coupling in JLV-APP-treated cells compared with the other three groups. Scale bar, 500 nm; green polygons mark ER-mitochondria contact sites. **F** ImageJ was used to quantitatively analyze the percentage of mitochondria membrane in contact with ER in four group cells. **G** Immunostaining for MFN2 in four group cells indicating an increased MFN2 fluorescence in JLV-APP-treated cells compared with the other three groups. Scale bar, 100 μm. **H** Western blot of MFN2 and ACAT1 to evaluate the MAM structure and activation in four group cells. **I** Quantitative analysis of optical densities of MFN2 and ACAT1 relative to GAPDH. ****$P < 0.0001$, ***$P < 0.001$ versus NC cells. All studies were performed independently at least three times

Cx43-Mediated MAM Formation Participates in the Pathological Changes in AD Cells

We subsequently prepared to explore whether Cx43-medicated MAM increase would contribute to the pathological changes in AD cells, mainly including Aβ42 deposition and neuronal apoptosis. We first studied the intracellular Aβ42 deposition via immunostaining. As shown in Fig. 6A, a few scattered spot-like intracellular Aβ42 fluorescence was observed in NC- and siRNA-treated cells, while a substantial amount of spot-like and even flaky intracellular Aβ42 fluorescence was found in JLV-APP- and siRNA + JLV-APP-treated cells, especially in JLV-APP-treated cells with more flaky intracellular Aβ42 fluorescence compared with siRNA + JLV-APP-treated cells. Western blot assay subsequently verified the results of Aβ42 immunostaining showing that the expression level of Aβ42 was obviously decreased in siRNA + JLV-APP-treated cells compared with JLV-APP-treated cells, and there was no significant difference between the other two groups (Fig. 6B, C). In addition to the direct cytotoxicity, intracellular Aβ42 aggregation can also be secreted from neuronal cells into extracellular space to form extracellular Aβ42 [46, 47]. Regarding the secreted Aβ42 alteration, an ELISA kit was used to determine the Aβ42 concentrations in the conditioned culture medium collected from the four cell groups. The concentration of Aβ42 in JLV-APP-treated cell culture was about twice that observed in siRNA + JLV-APP-treated cell culture, the latter of which had no significant difference with the NC- and siRNA-treated cells (Fig. 6D). Thereby, we identify that MAM decrease caused by Cx43 deficiency can significantly

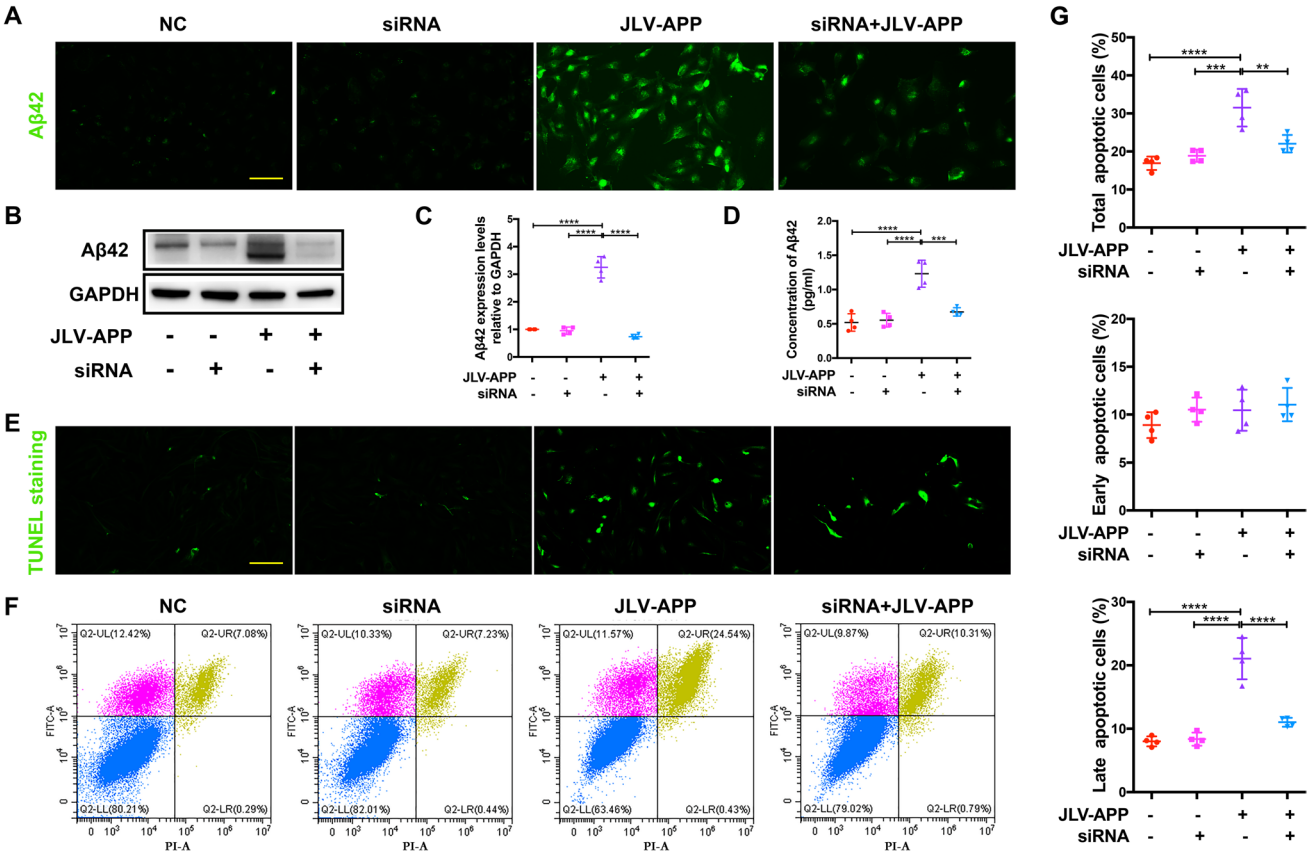

Fig. 6 Cx43-mediated MAM formation in AD cells promotes Aβ42 deposition and neuronal apoptosis. **A** Representative images depicting immunofluorescent labeling Aβ42 in the four cell groups. Scale bar, 100 μm. **B** Western blot analysis for Aβ42 expression of samples from the four cell groups. **C** Quantitative analysis of Aβ42 relative to GAPDH was performed. **D** Aβ42 concentrations in the culture medium of four cell groups were analyzed using an Aβ42 ELISA kit. **E** TUNEL staining was performed to evaluate the neuronal apoptosis in four cell groups. Scale bar, 100 μm. **F** An apoptosis assay was performed via flow cytometry after Annexin V-FITC/PI double staining. Viable cells appeared in the lower left quadrant, early apoptotic cells were presented in the upper left quadrant, and late apoptotic cells were shown in the upper right quadrant. **G** Quantitative analysis of the percentage of viable cells, early apoptotic cells, and late apoptotic cells. ****$P < 0.0001$, ***$P < 0.001$, **$P < 0.01$ versus NC cells. All studies were performed independently at least three times

reduce both the intracellular and extracellular Aβ aggregation in vitro.

Neuronal apoptosis is another major pathological feature in AD. The TUNEL analysis of cells revealed that sporadic apoptotic cells appeared in the NC- and Cx43 siRNA-treated groups, while numerous apoptotic fluorescence signals were observed in JLV-APP-treated cells, which can be largely alleviated via Cx43 siRNA treatment for JLV-APP-treated cells (Fig. 6E). Additionally, the cells were doubly stained with Annexin V-FITC and PI to further investigate the apoptotic states of cells via flow cytometry. On the flow cytometry charts in Fig. 6F, cells were divided into four categories: viable cells (Annexin V^-/PI^-), early apoptotic cells (Annexin V^+/PI^-), late apoptotic cells (Annexin V^+/PI^+), and necrotic cells (Annexin V^-/PI^+). The flow cytometric analysis demonstrated that approximately 80% of cells were viable in the NC-, siRNA-, and siRNA + JLV-APP-treated cell groups, while only about 60% of cells in JLV-APP-treated cell groups (Fig. 6F). The statistical analysis of the percentage of apoptotic cells revealed that there was no significant difference of early apoptotic cells among these four cell groups, but the late apoptotic cells were dramatically increased to about 25% in JLV-APP-treated cell groups compared with the other three cell groups with only 10% late apoptotic cells at most (Fig. 6G), which demonstrated that Cx43-mediated MAM formation promoted the neuronal apoptosis mainly through affecting the late apoptosis progress. Taken together, MAM formation participates in the pathological changes in AD cells, mainly including Aβ42 deposition and neuronal apoptosis, which can be attenuated by inhibiting Cx43 expression to decrease MAM structure.

MAM Regulates Autophagy Inhibition in an mTOR-Dependent Pathway In Vitro

To explore whether the underlying mechanism of the above pathological changes in AD cells is associated with

autophagy like that in vivo, we first observed the cellular microstructure through the TEM technique. As shown in Fig. 7A, only a few autophagosomes (black arrows) were found in the first three cell groups, and even fewer in the JLV-APP-treated cells, whereas many autophagosomes (black arrows) were found in the siRNA + JLV-APP-treated cells. Namely, autophagy is likely to be activated in siRNA + JLV-APP-treated cells, although it was impaired in JLV-APP-treated cells. Consistent with the findings in vivo, the double immunostaining for P62 and LC3B subsequently revealed the colocalization of P62 with LC3B puncta in JLV-APP-treated cells was obviously less than that in

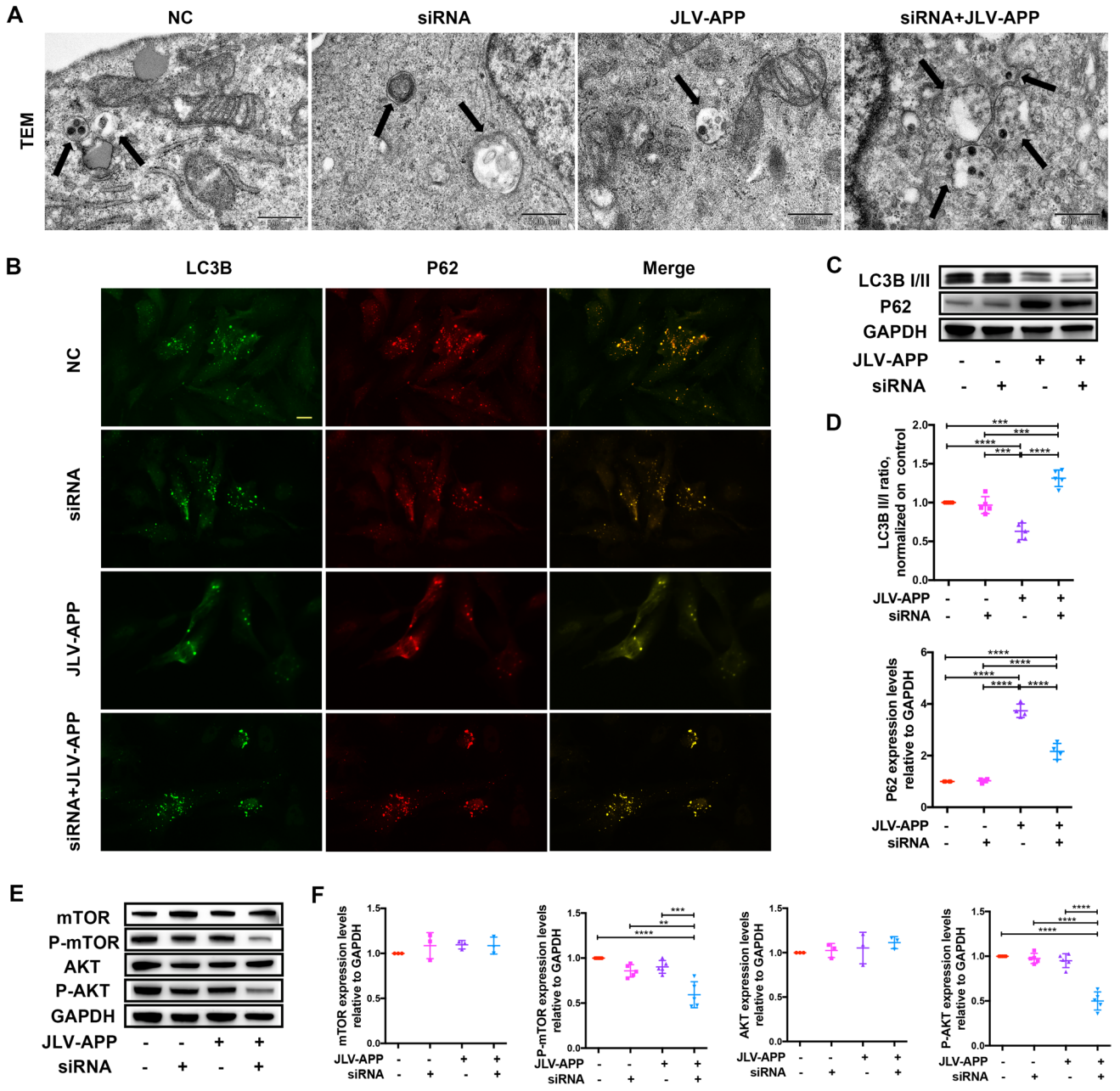

Fig. 7 Cx43-mediated MAM generation negatively regulates autophagy through activating mTOR-dependent pathway in AD cells. **A** Representative electron micrographs of autophagosome structures (black arrows) in four cell groups. Scale bar, 500 nm. **B** Representative images of double immunostaining for LC3B (green) and P62 (red) in four cell groups. Scale bar, 50 μm. **C** Western blot analysis for LC3B and P62 expressions to evaluate autophagic flux in four cell groups, and GAPDH was an internal control. **D** Quantitative analysis of LC3B and P62 relative to GAPDH. **E** Representative images of a western blot for proteins related to mTOR-dependent signaling pathway in four cell groups. **F** Quantitative analysis of the band intensities of proteins related to mTOR-dependent signaling pathway. $^{****}P < 0.0001$, $^{***}P < 0.001$, $^{**}P < 0.01$ versus NC cells. All studies were performed independently at least three times

siRNA + JLV-APP-treated cells, and the fluorescence intensities were also relatively weaker in JLV-APP-treated cells than that in the other three cell groups without the significant difference of fluorescence colocalization observed (Fig. 7B). Meanwhile, the western blot results showed that the expression levels of both LC3B-I and LC3B-II form in JLV-APP- and siRNA + JLV-APP-treated cells were lower than that in NC- and siRNA-treated cells, but the predominant form of LC3B detected was different (Fig. 7C, D). LC3B mainly existed in the form of LC3B-II in siRNA + JLV-APP-treated cells while LC3B-I in JLV-APP-treated cells (Fig. 7C), and the ration of LC3BII/I in siRNA + JLV-APP-treated cells was almost twice that in JLV-APP-treated cells (Fig. 7D), which demonstrated that there was a more activated autophagy flux in siRNA + JLV-APP-treated cells than that in JLV-APP-treated cells, although the autophagy activities of cells in both groups were impaired. Simultaneously, the expression levels of P62 in JLV-APP- and siRNA + JLV-APP-treated cells were higher than that in NC- and siRNA-treated cells, especially in JLV-APP-treated cells (Fig. 7C, D), which together with the conversion of LC3B verified a more activated autophagy flux in siRNA + JLV-APP-treated cells than JLV-APP-treated cells.

Finally, we performed a western blot assay to confirm the mTOR-dependent signaling pathway involved in the MAM-induced autophagy inhibition *in vitro*. In line with the results *in vivo*, western blot analysis *in vitro* showed that there was no difference in total mTOR and AKT expression levels among these four cell groups, while the expression levels of P-mTOR and P-AKT were obviously lower in siRNA + JLV-APP-treated cells than that in the other three cell groups with no significant difference found (Fig. 7E, F). These results *in vitro* validate that the Cx43-mediated MAM formation can negatively regulate the autophagy functions in AD cells through activating the mTOR-dependent pathway, which can be reversed by Cx43 siRNA treatment.

Discussion

As the most abundant gap junction (GJ) protein in the brain, Cx43 has been found to be critically involved in the pathogenesis of neurodegenerative diseases. Therefore, the involvement of Cx43 in AD pathogenesis also gradually becomes an appealing research area expanding vigorously in recent decades. It has been proved that Cx43 immunoreactivity is evidently increased in AD postmortem brains and mouse models [28, 48], promoting the AD pathogenesis through various pathogenic mechanisms. Consistent with but beyond these studies, we hypothesize and validate not only the upregulation of Cx43 expression in the AD mouse model but also its regulatory role in driving a large MAM-specific molecular network underlying AD. In detail, four major findings were drawn from this work. Firstly, we have confirmed first that Cx43 is a major player in the MAM formation, and the upregulation of Cx43 can significantly increase the contact sites between the ER and mitochondria in AD mice and cells. Secondly, Cx43-mediated MAM formation can subsequently contribute to the key neuropathological features that characterize all AD brains, mainly including Aβ deposition, reactive astrogliosis, and neuronal apoptosis, which exactly explains why neurons and synapses are losing in AD brains. Thirdly, Aβ deposition and Aβ-associated pathological changes are mainly due to the negative autophagy regulation of Cx43-mediated MAM formation through activating the mTOR-dependent signaling pathway. Finally, Cx43 knockout or siRNA treatment significantly reduces the MAM structure and then promotes Aβ clearance via triggering the mTOR-dependent autophagy, ultimately attenuating Aβ deposition and Aβ-associated pathological alterations in AD mice and cells. Taken together, this work thus provides the novel insights into the cellular mechanism by which Cx43 causes AD pathogenesis, rather than the conventional channel functions of Cx43, the thorough comprehension of which plays a vital role in exploring an alternative therapeutic strategy targeting Cx43 non-channel functions in AD.

Cx43 usually exists in the form of GJ that is the cluster of a few tens to thousands of cell-to-cell channels and mediates gap junction intercellular communication (GJIC) by allowing the direct intercellular exchange of small molecules up to approximately 1.5 kDa in size [49]. A single GJ comprises two opposing specialized cell-to-cell connexon channels formed by oligomerization of six Cx43 proteins [50]. Additionally, connexon also does exist independently as the single membrane channel, commonly named hemichannel. Hemichannel keeps a low opening probability under normal condition to mediate the interaction between cells and extracellular space [51], but is usually open when triggered by various pathological situations, such as Aβ aggregation and inflammatory in AD. The opening of the hemichannel allows numerous small molecules like adenosine triphosphate (ATP) and glutamate to be released into extracellular space [52], which is commonly considered deleterious due to the potential cytoplasmic impairment and neurotoxic damage [53]. Accumulating evidence indicates that the GJ and hemichannel function are closely associated with the onset and progression of neurodegenerative diseases. For example, Cx43-associated GJIC is impaired, while activated hemichannel opening is increased significantly maintaining a sustained gliotransmitter release to amplify neuronal toxicity, both of them ultimately contribute to cognitive impairment in AD [54]. Thus, the function of Cx43 GJ and hemichannel play important roles in the pathogenesis of AD and has become the focus of connexin research in the past decades, thus ignoring the non-channel function of

the Cx43 cytosolic C-terminus. The cytosolic C-terminus of Cx43 participates in protein interactions via its multiple domains that endow Cx43 with the channel-independent abilities of influencing cell growth and differentiation [55]. In our study, we have revealed that Cx43 plays an important role in regulating the MAM structure without the channel-dependent function in AD. Cx43 deficiency appears to mitigate the increase of MAM in AD, while has no effect on MAM structure in normal mice and cells. Notably, we provide the first preliminary evidence to support the view that Cx43 is a major contributor to the MAM formation. Increased MAM formation is usually accompanied by the perturbed MAM functions, mainly including calcium dysregulation, ascended lipid level, mitochondrial dysfunction, oxidative stress, and autophagy, all of which are involved in the AD onset and progression and precede the appearance of plaques and tangles [56]. Thus, the MAM hypothesis is naturally identified as the fundamental for the biochemical and morphological phenotypes in AD, instead of the amyloid cascade hypothesis, due to the fact that it can accurately explain the early pathological alternations discovered in both familial and sporadic AD. The MAM hypothesis does not negate the amyloid cascade hypothesis, but rather emphasizes that plaques and tangles are not causes, but indeed the final consequences of AD pathogenesis. What makes sense is that we have first figured out the biochemical upstream molecule causing the ER-mitochondrial hyper-connectivity and perturbed MAM function, which may be viable as a novel potential drug target for AD treatment. However, it is unfortunate that we have not been able to determine the precise molecular mechanism of Cx43 regulating MAM formation, which is necessary to be delineated through further studies. Only by clarifying the underlying mechanism of Cx43 regulating MAM formation can we better provide accurate therapeutic targets for AD.

Furthermore, we have revealed that Cx43-mediated MAM formation contributes to the neuropathological changes in AD, such as Aβ deposition, reactive astrogliosis, and neuronal apoptosis, which can be ameliorated by Cx43 knockout or siRNA inhibition. Our findings are consistent with those obtained from the previous studies demonstrating the protective effects of Cx43 reduction on Aβ-related pathological changes in AD [57]. Conversely, Aβ aggregation can significantly impair Cx43 GJIC function and promote hemichannel activities in astrocytes [58]. One consequence of this vicious circle involving Cx43 and Aβ is a chronic activation of Cx43 hemichannel that represents a pathway for ATP and glutamate efflux [59], which jointly contributes to the AD pathogenesis. MAM, as the downstream of Cx43, is also involved in this vicious circuit. Numerous studies have demonstrated that the PS1/2 and γ-secretase enzymes are localized not only at the plasma membrane but also predominantly at MAM [60]. PS1/2 and γ-secretase enzymes located at MAM play critical roles in the generation of intracellular Aβ, with OMM serving as an Aβ translocase machinery to the cristae membrane in mitochondria [61]. Mitochondrial Aβ deposition, significantly observed in AD postmortem brains and mouse models, can thereby contribute to extracellular Aβ deposition, both of which would negatively affect neuron functions and even result in cognitive impairment [62, 63]. Therefore, Cx43-mediated MAM increase can promote both intracellular and even extracellular Aβ deposition as shown in Fig. 7, which magnifies the neurotoxic effect and then leads to the neuronal apoptosis. Additionally, Aβ exposure for neurons, in turn, can also increase the contact points between ER and mitochondria, which indicates that MAM augment is observed not only at pathological conditions such as in early AD but also after exposure to Aβ [64]. Nevertheless, whether Aβ increase directly leads to the MAM augment or indirectly by affecting Cx43 expression needs to be established in future studies. Anyhow, both Cx43 and MAM interventions can alleviate the pathological changes of AD. However, in contrast with the above-described studies showing the key role of Cx43 in Aβ generation, a number of studies have shown that Cx43 has no effect on the formation of Aβ plaque, and the specific deletion of astrocytic Cx43 in APP/PS1 mice mainly attenuates cognitive impairment through decreasing astrogliosis and increasing synaptic function without affection on Aβ formation [57]. Meanwhile, there are even studies showing that Cx43 has important neuroprotective effects for AD, and the maintenance of Cx43 expression in astrocyte contributes to prevent neurons from damages in response to various harmful stimuli [65]. Accordingly, both the memory benefit and deteriorating function of astrocytes-located Cx43 have been documented, which may be due to a variety of factors. Firstly, Cx43 itself has the opposite biological functions. The physiologically expressed Cx43 mainly contributes to memory formation, while pathologically increased Cx43 expression may be involved in neuronal damage and cognitive impairment. Consequently, there is likely a balance between beneficial and deteriorating signaling in neurons due to the expression ratio of these two properties of Cx43, which ultimately determines to mitigate or promote the neurodegenerative processes, the key step of neurotoxicity for death. Next, Aβ-related pathological changes are in varying degrees during the different stages of AD, which makes Cx43 in distinct conditions of physiological or pathological states. For example, in the early stage of AD, less aggregated Aβ stimulates Cx43 hemichannel-mediated release of glutathione, the major antioxidant in the central nervous system, from astrocytes to prevent neurons from oxidative stress damage [66]. However, Cx43 hemichannel opening generally promotes pathological changes in the other stages of AD. Finally, studies on the underlying mechanism of Cx43-induced AD pathogenesis involve various cell types mainly

including astrocyte, neuron, and fibroblast, and different expression levels and functions of Cx43 in these cells may produce inconsistent results due to its opposite biological functions. Therefore, it is difficult to define whether Cx43 must mitigate or promote Aβ formation and Aβ-associated neuropathological changes, and further experiments will be necessary to better figure out the causes of this discrepancy.

In our study, Aβ deposition and Aβ-related pathological alternations in AD are mainly attributable to the upregulation of MAM function, which is characterized by the negative regulation of autophagy via initiating mTOR-dependent pathway. Our finding that Cx43 negatively modulates autophagy is consistent with the results from previous studies [67]. Cells lacking Cx43 show an obvious increase in autophagic vacuoles and higher autophagic fluxes of LC3, which suggests that Cx43 deficiency gives rise to the constitutive autophagy activation mainly through increasing biogenesis rather than reducing lysosomal clearance [68]. Conversely, Cx43 overexpression will consistently attenuate autophagic flux. Notably, due to the critical role of Cx43 in GJIC, the potent GJ inhibitor 18α glycyrrhetinic acid is used to explore whether autophagy upregulation can be recapitulated, and the result indicates no alternation in Cx43-associated autophagosome structure and even a decreased autophagic flux that is contrast to Cx43 ablation [68]. GJ inhibition experiment further confirms that the Cx43-mediated negative effect on autophagy does not depend on its GJIC role, but on the non-channel function of the Cx43 C-terminus. However, the mechanism of Cx43 non-channel function-mediated autophagy inhibition is still poorly understood. In this context, we reveal that MAM is involved in Cx43-mediated autophagy inhibition. As described earlier, Cx43 can facilitate the MAM formation, while MAM is rich in ACAT1 protein. Previous studies have revealed that both ACAT1 gene knockout and pharmacological inhibition can significantly promote the autophagosome generation and lysosomal proteolysis without affecting the total cell cholesterol content, which indicates that ACAT1 blockage may initiate autophagy through increasing the local cholesterol level in MAM [69]. Thus, the negative regulation of autophagy induced by Cx43-mediated MAM increase may be primarily achieved through the abundant ACAT1 protein in MAM. However, the necessity of ACAT1 in MAM-induced autophagy inhibition and the alterations of the local cholesterol level in increased MAM in our studies also need additional investigation. Additionally, it is worth noting that the augmented MAM can initiate the mTOR-dependent pathway to participate in negatively regulating autophagy, which is consistent with existing researches that the complicated mTOR-dependent pathway is involved in AD pathology via autophagic regulation [70]. However, we cannot rule out the involvement of other autophagic regulation pathways in the MAM-induced autophagy inhibition, such as the mTOR-independent signaling pathway [71]. Thus, further experiments are necessary for a more throughout understanding about the signaling transduction pathway involved in MAM-induced autophagy inhibition, which will be benefit for any future new experiment designs and clinical trials for AD. Additionally, there are still some limitations in this study. Mice with global Cx43 homozygous deficiency cannot be used because they die perinatally owing to an obstruction of the right ventricular outflow tract of the heart. Cx43 heterozygous mice still express some amount of Cx43 protein. On the other hand, Cx43 is also expressed in other cell types mainly including endothelial cells, pericytes, and astrocytes. Thus, further research is needed to understand the influence of Cx43-associated MAM alteration on AD in these types of cells. In particular, the use of cell-specific Cx43 knockout mice could be helpful to validate the results of our study.

Conclusion

Taken together, our findings support the previously unrecognized view that Cx43 non-channel function also plays a key role in AD pathogenesis through upregulating MAM formation and function. Increased MAM formation shown here contributes to the negative regulation of autophagy via activating the mTOR-dependent pathway, which results in the obvious Aβ deposition and neuronal apoptosis. The deficiency of Cx43 reduces Aβ-associated neuropathological alternations through downregulating MAM formation and its autophagy inhibition function. However, the precise molecular mechanism of Cx43 regulating MAM formation is currently unclear, and work to elucidate the underlying mechanism by which Cx43 contributes to MAM formation is currently under way. Even so, this study still presents a complete characterization of these processes, which may provide the novel insights into the cellular mechanisms by which Cx43 affects AD pathogenesis and then help to develop the therapeutic strategies with the purpose of restoring neuronal homeostasis.

Author Contribution Weiwei Yu and Yunong Li were involved in designing this study, analyzing and interpreting these results, and drafting and revising this manuscript. Yao Li participated in analyzing these data and revising the manuscript. Jun Hu was involved in designing the study and revising this manuscript. Jun Wu participated in the concept and design of this study and obtained funding. Xuhui Chen contributed toward analyzing these data and revising this manuscript. Xin Shi was involved in designing this study and analyzing these results. Yining Huang was involved in revising this manuscript and providing the funding support.

Funding This work was supported by the National Natural Science Foundation of China [NSFC: 81971115, 32300982] and the Science,

Technology, and Innovation Commission of Shenzhen Municipality [SGLH20180629094602262].

Data Availability All the data generated during this study are available from the corresponding authors on reasonable request. Source data are provided in this paper.

Declarations

Ethics Approval and Consent to Participate All experiments with animals were approved by Peking University Shenzhen Hospital and complied with the ethics approval obtained from Peking University Shenzhen Hospital (the specific ethics batch number: 2023–271) as well as the National Institutes of Health Guide for the Care and Use of Laboratory Animals.

Consent for Publication Yes, all the authors have given their consent for the publication of this manuscript in its present form.

Competing Interests The authors declare no competing interests.

References

1. Skaper SD (2012) Alzheimer's disease and amyloid: culprit or coincidence? Int Rev Neurobiol 102:277–316. https://doi.org/10.1016/b978-0-12-386986-9.00011-9
2. Baumgart M, Snyder HM, Carrillo MC, Fazio S, Kim H, Johns H (2015) Summary of the evidence on modifiable risk factors for cognitive decline and dementia: a population-based perspective. Alzheimers Dement 11(6):718–726. https://doi.org/10.1016/j.jalz.2015.05.016
3. Lane CA, Hardy J, Schott JM (2018) Alzheimer's disease. Eur J Neurol 25(1):59–70. https://doi.org/10.1111/ene.13439
4. Barage SH, Sonawane KD (2015) Amyloid cascade hypothesis: pathogenesis and therapeutic strategies in Alzheimer's disease. Neuropeptides 52:1–18. https://doi.org/10.1016/j.npep.2015.06.008
5. Hardy JA, Higgins GA (1992) Alzheimer's disease: the amyloid cascade hypothesis. Science 256(5054):184–185. https://doi.org/10.1126/science.1566067
6. Weller J, Budson A (2018) Current understanding of Alzheimer's disease diagnosis and treatment. F1000Res 7:1161. https://doi.org/10.12688/f1000research.14506.1
7. Bateman RJ, Aisen PS, De Strooper B, Fox NC, Lemere CA, Ringman JM, Salloway S, Sperling RA et al (2011) Autosomal-dominant Alzheimer's disease: a review and proposal for the prevention of Alzheimer's disease. Alzheimers Res Ther 3(1):1. https://doi.org/10.1186/alzrt59
8. Bezprozvanny I, Mattson MP (2008) Neuronal calcium mishandling and the pathogenesis of Alzheimer's disease. Trends Neurosci 31(9):454–463. https://doi.org/10.1016/j.tins.2008.06.005
9. Pettegrew JW, Panchalingam K, Hamilton RL, McClure RJ (2001) Brain membrane phospholipid alterations in Alzheimer's disease. Neurochem Res 26(7):771–782. https://doi.org/10.1023/a:1011603916962
10. Stefani M, Liguri G (2009) Cholesterol in Alzheimer's disease: unresolved questions. Curr Alzheimer Res 6(1):15–29. https://doi.org/10.2174/156720509787313899
11 Wang X, Su B, Zheng L, Perry G, Smith MA, Zhu X (2009) The role of abnormal mitochondrial dynamics in the pathogenesis of Alzheimer's disease. J Neurochem 109(Suppl 1):153–159. https://doi.org/10.1111/j.1471-4159.2009.05867.x
12. Friedman JR, Lackner LL, West M, DiBenedetto JR, Nunnari J, Voeltz GK (2011) ER tubules mark sites of mitochondrial division. Science 334(6054):358–362. https://doi.org/10.1126/science.1207385
13. Janikiewicz J, Szymański J, Malinska D, Patalas-Krawczyk P, Michalska B, Duszyński J, Giorgi C, Bonora M et al (2018) Mitochondria-associated membranes in aging and senescence: structure, function, and dynamics. Cell Death Dis 9(3):332. https://doi.org/10.1038/s41419-017-0105-5
14. de Brito OM, Scorrano L (2008) Mitofusin 2 tethers endoplasmic reticulum to mitochondria. Nature 456(7222):605–610. https://doi.org/10.1038/nature07534
15. Shi W, Wu H, Liu S, Wu Z, Wu H, Liu J, Hou Y (2021) Progesterone suppresses cholesterol esterification in APP/PS1 mice and a cell model of Alzheimer's disease. Brain Res Bull 173:162–173. https://doi.org/10.1016/j.brainresbull.2021.05.020
16. Szymański J, Janikiewicz J, Michalska B, Patalas-Krawczyk P, Perrone M, Ziółkowski W, Duszyński J, Pinton P et al (2017) Interaction of mitochondria with the endoplasmic reticulum and plasma membrane in calcium homeostasis, lipid trafficking and mitochondrial structure. Int J Mol Sci 18(7):1576. https://doi.org/10.3390/ijms18071576
17. Area-Gomez E, Del Carmen Lara Castillo M, Tambini MD, Guardia-Laguarta C, de Groof AJ, Madra M, Ikenouchi J, Umeda M et al (2012) Upregulated function of mitochondria-associated ER membranes in Alzheimer disease. Embo J 31(21):4106–4123. https://doi.org/10.1038/emboj.2012.202
18. Hedskog L, Pinho CM, Filadi R, Rönnbäck A, Hertwig L, Wiehager B, Larssen P, Gellhaar S et al (2013) Modulation of the endoplasmic reticulum-mitochondria interface in Alzheimer's disease and related models. Proc Natl Acad Sci USA 110(19):7916–7921. https://doi.org/10.1073/pnas.1300677110
19. Moorer MC, Stains JP (2017) Connexin43 and the intercellular signaling network regulating skeletal remodeling. Curr Osteoporos Rep 15(1):24–31. https://doi.org/10.1007/s11914-017-0345-4
20. Wang M, Smith K, Yu Q, Miller C, Singh K, Sen CK (2019) Mitochondrial connexin 43 in sex-dependent myocardial responses and estrogen-mediated cardiac protection following acute ischemia/reperfusion injury. Basic Res Cardiol 115(1):1. https://doi.org/10.1007/s00395-019-0759-5
21. Maulik M, Vasan L, Bose A, Dutta Chowdhury S, Sengupta N, Das Sarma J (2020) Amyloid-β regulates gap junction protein connexin 43 trafficking in cultured primary astrocytes. J Biol Chem 295(44):15097–15111. https://doi.org/10.1074/jbc.RA120.013705
22. He J, Gong M, Wang Z, Liu D, Xie B, Luo C, Li G, Tse G et al (2021) Cardiac abnormalities after induction of endoplasmic reticulum stress are associated with mitochondrial dysfunction and connexin43 expression. Clin Exp Pharmacol Physiol 48(10):1371–1381. https://doi.org/10.1111/1440-1681.13541

23. Lv Y, Cheng L, Peng F (2022) Compositions and functions of mitochondria-associated endoplasmic reticulum membranes and their contribution to cardioprotection by exercise preconditioning. Front Physiol 13:910452. https://doi.org/10.3389/fphys.2022.910452
24. Barac YD, Zeevi-Levin N, Yaniv G, Reiter I, Milman F, Shilkrut M, Coleman R, Abassi Z et al (2005) The 1,4,5-inositol trisphosphate pathway is a key component in Fas-mediated hypertrophy in neonatal rat ventricular myocytes. Cardiovasc Res 68(1):75–86. https://doi.org/10.1016/j.cardiores.2005.05.015
25. Zou H, Zhuo L, Han T, Hu D, Yang X, Wang Y, Yuan Y, Gu J et al (2015) Autophagy and gap junctional intercellular communication inhibition are involved in cadmium-induced apoptosis in rat liver cells. Biochem Biophys Res Commun 459(4):713–719. https://doi.org/10.1016/j.bbrc.2015.03.027
26. Kang M, Lin N, Li C, Meng Q, Zheng Y, Yan X, Deng J, Ou Y et al (2014) Cx43 phosphorylation on S279/282 and intercellular communication are regulated by IP3/IP3 receptor signaling. Cell Commun Signal 12:58. https://doi.org/10.1186/s12964-014-0058-6
27. Yi C, Mei X, Ezan P, Mato S, Matias I, Giaume C, Koulakoff A (2016) Astroglial connexin43 contributes to neuronal suffering in a mouse model of Alzheimer's disease. Cell Death Differ 23(10):1691–1701. https://doi.org/10.1038/cdd.2016.63
28. Nagy JI, Li W, Hertzberg EL, Marotta CA (1996) Elevated connexin43 immunoreactivity at sites of amyloid plaques in Alzheimer's disease. Brain Res 717(1–2):173–178. https://doi.org/10.1016/0006-8993(95)01526-4
29. Fong JT, Kells RM, Gumpert AM, Marzillier JY, Davidson MW, Falk MM (2012) Internalized gap junctions are degraded by autophagy. Autophagy 8(5):794–811. https://doi.org/10.4161/auto.19390
30. Tubbs E, Chanon S, Robert M, Bendridi N, Bidaux G, Chauvin MA, Ji-Cao J, Durand C et al (2018) Disruption of mitochondria-associated endoplasmic reticulum membrane (MAM) integrity contributes to muscle insulin resistance in mice and humans. Diabetes 67(4):636–650. https://doi.org/10.2337/db17-0316
31. Lokossou AG, Toufaily C, Vargas A, Barbeau B (2016) siRNA transfection and EMSA analyses on freshly isolated human villous cytotrophoblasts. J Vis Exp (115). https://doi.org/10.3791/53995
32. Filadi R, Greotti E, Pizzo P (2018) Highlighting the endoplasmic reticulum-mitochondria connection: focus on mitofusin 2. Pharmacol Res 128:42–51. https://doi.org/10.1016/j.phrs.2018.01.003
33. Yu W, Jin H, Huang Y (2021) Mitochondria-associated membranes (MAMs): a potential therapeutic target for treating Alzheimer's disease. Clin Sci (Lond) 135(1):109–126. https://doi.org/10.1042/cs20200844
34. Grinberg LT, Thal DR (2010) Vascular pathology in the aged human brain. Acta Neuropathol 119(3):277–290. https://doi.org/10.1007/s00401-010-0652-7
35. van Westen D, Lindqvist D, Blennow K, Minthon L, Nägga K, Stomrud E, Zetterberg H, Hansson O et al (2016) Cerebral white matter lesions - associations with Aβ isoforms and amyloid PET. Sci Rep 6:20709. https://doi.org/10.1038/srep20709
36. Chen Y, Aulia S, Tang BL (2006) Myelin-associated glycoprotein-mediated signaling in central nervous system pathophysiology. Mol Neurobiol 34(2):81–91. https://doi.org/10.1385/mn:34:2:81
37. Zhou F, van Laar T, Huang H, Zhang L (2011) APP and APLP1 are degraded through autophagy in response to proteasome inhibition in neuronal cells. Protein Cell 2(5):377–383. https://doi.org/10.1007/s13238-011-1047-9
38. Son SM, Jung ES, Shin HJ, Byun J, Mook-Jung I (2012) Aβ-induced formation of autophagosomes is mediated by RAGE-CaMKKβ-AMPK signaling. Neurobiol Aging 33(5):1006.e1011-1023. https://doi.org/10.1016/j.neurobiolaging.2011.09.039
39 Reddy PH, Oliver DM (2019) Amyloid beta and phosphorylated Tau-induced defective autophagy and mitophagy in Alzheimer's disease. Cells 8(5):448. https://doi.org/10.3390/cells8050488
40. Komatsu M, Kageyama S, Ichimura Y (2012) p62/SQSTM1/A170: physiology and pathology. Pharmacol Res 66(6):457–462. https://doi.org/10.1016/j.phrs.2012.07.004
41. Fischer TD, Wang C, Padman BS, Lazarou M, Youle RJ (2020) STING induces LC3B lipidation onto single-membrane vesicles via the V-ATPase and ATG16L1-WD40 domain. J Cell Biol 219 (12). https://doi.org/10.1083/jcb.202009128
42. Tiberti M, Di Leo L, Vistesen MV, Kuhre RS, Cecconi F, De Zio D, Papaleo E (2022) The Cancermuts software package for the prioritization of missense cancer variants: a case study of AMBRA1 in melanoma. Cell Death Dis 13(10):872. https://doi.org/10.1038/s41419-022-05318-2
43. Jiang P, Mizushima N (2015) LC3- and p62-based biochemical methods for the analysis of autophagy progression in mammalian cells. Methods 75:13–18. https://doi.org/10.1016/j.ymeth.2014.11.021
44. Pei JJ, Hugon J (2008) mTOR-dependent signalling in Alzheimer's disease. J Cell Mol Med 12(6b):2525–2532. https://doi.org/10.1111/j.1582-4934.2008.00509.x
45. Caccamo A, Maldonado MA, Majumder S, Medina DX, Holbein W, Magrí A, Oddo S (2011) Naturally secreted amyloid-beta increases mammalian target of rapamycin (mTOR) activity via a PRAS40-mediated mechanism. J Biol Chem 286(11):8924–8932. https://doi.org/10.1074/jbc.M110.180638
46. Fernández-Vizarra P, Fernández AP, Castro-Blanco S, Serrano J, Bentura ML, Martínez-Murillo R, Martínez A, Rodrigo J (2004) Intra- and extracellular Abeta and PHF in clinically evaluated cases of Alzheimer's disease. Histol Histopathol 19(3):823–844. https://doi.org/10.14670/hh-19.823
47. Blanchard V, Moussaoui S, Czech C, Touchet N, Bonici B, Planche M, Canton T, Jedidi I et al (2003) Time sequence of maturation of dystrophic neurites associated with Abeta deposits in APP/PS1 transgenic mice. Exp Neurol 184(1):247–263. https://doi.org/10.1016/s0014-4886(03)00252-8
48. Mei X, Ezan P, Giaume C, Koulakoff A (2010) Astroglial connexin immunoreactivity is specifically altered at β-amyloid plaques in β-amyloid precursor protein/presenilin1 mice. Neuroscience 171(1):92–105. https://doi.org/10.1016/j.neuroscience.2010.08.001
49. Yu W, Jin H, Sun W, Nan D, Deng J, Jia J, Yu Z, Huang Y (2021) Connexin43 promotes angiogenesis through activating the HIF-1α/VEGF signaling pathway under chronic cerebral hypoperfusion. J Cerebral Blood Flow Metabolism : Off J Int Society Cerebral Blood Flow Metabolism 41(10):2656–2675. https://doi.org/10.1177/0271678x211010354
50. Kajiwara Y, Wang E, Wang M, Sin WC, Brennand KJ, Schadt E, Naus CC, Buxbaum J et al (2018) GJA1 (connexin43) is a key regulator of Alzheimer's disease pathogenesis. Acta Neuropathol Commun 6(1):144. https://doi.org/10.1186/s40478-018-0642-x
51. He JT, Li XY, Yang L, Zhao X (2020) Astroglial connexins and cognition: memory formation or deterioration? Biosci Rep 40 (1). https://doi.org/10.1042/bsr20193510
52. Abudara V, Roux L, Dallérac G, Matias I, Dulong J, Mothet JP, Rouach N, Giaume C (2015) Activated microglia impairs neuroglial interaction by opening Cx43 hemichannels in hippocampal astrocytes. Glia 63(5):795–811. https://doi.org/10.1002/glia.22785
53. Giaume C, Leybaert L, Naus CC, Sáez JC (2013) Connexin and pannexin hemichannels in brain glial cells: properties, pharmacology, and roles. Front Pharmacol 4:88. https://doi.org/10.3389/fphar.2013.00088
54. Gajardo-Gomez R, Labra VC, Maturana CJ, Shoji KF, Santibanez CA, Saez JC, Giaume C, Orellana JA (2017) Cannabinoids prevent

the amyloid beta-induced activation of astroglial hemichannels: a neuroprotective mechanism. Glia 65(1):122–137. https://doi.org/10.1002/glia.23080
55. Leithe E, Mesnil M (1860) Aasen T (2018) The connexin 43 C-terminus: a tail of many tales. Biochim Biophys Acta Biomembr 1:48–64. https://doi.org/10.1016/j.bbamem.2017.05.008
56. Area-Gomez E, Schon EA (2017) Alzheimer disease. Adv Exp Med Biol 997:149–156. https://doi.org/10.1007/978-981-10-4567-7_11
57. Ren R, Zhang L, Wang M (2018) Specific deletion connexin43 in astrocyte ameliorates cognitive dysfunction in APP/PS1 mice. Life Sci 208:175–191. https://doi.org/10.1016/j.lfs.2018.07.033
58. Orellana JA, Shoji KF, Abudara V, Ezan P, Amigou E, Sáez PJ, Jiang JX, Naus CC et al (2011) Amyloid β-induced death in neurons involves glial and neuronal hemichannels. J Neurosci : Off J Soc Neurosci 31(13):4962–4977. https://doi.org/10.1523/jneurosci.6417-10.2011
59. Stridh MH, Tranberg M, Weber SG, Blomstrand F, Sandberg M (2008) Stimulated efflux of amino acids and glutathione from cultured hippocampal slices by omission of extracellular calcium: likely involvement of connexin hemichannels. J Biol Chem 283(16):10347–10356. https://doi.org/10.1074/jbc.M704153200
60. Area-Gomez E, Schon EA (2017) On the pathogenesis of Alzheimer's disease: the MAM hypothesis. Faseb j 31(3):864–867. https://doi.org/10.1096/fj.201601309
61. Pinho CM, Teixeira PF (1837) Glaser E (2014) Mitochondrial import and degradation of amyloid-β peptide. Biochem Biophys Acta 7:1069–1074. https://doi.org/10.1016/j.bbabio.2014.02.007
62. Fang D, Wang Y, Zhang Z, Du H, Yan S, Sun Q, Zhong C, Wu L et al (2015) Increased neuronal PreP activity reduces Aβ accumulation, attenuates neuroinflammation and improves mitochondrial and synaptic function in Alzheimer disease's mouse model. Hum Mol Genet 24(18):5198–5210. https://doi.org/10.1093/hmg/ddv241
63. Caspersen C, Wang N, Yao J, Sosunov A, Chen X, Lustbader JW, Xu HW, Stern D et al (2005) Mitochondrial Abeta: a potential focal point for neuronal metabolic dysfunction in Alzheimer's disease. Faseb j 19(14):2040–2041. https://doi.org/10.1096/fj.05-3735fje
64. Nikolaeva NS, Yandulova EY, Aleksandrova YR, Starikov AS, Neganova ME (2022) The role of a pathological interaction between β-amyloid and mitochondria in the occurrence and development of Alzheimer's disease. Acta Naturae 14(3):19–34. https://doi.org/10.32607/actanaturae.11723
65. Majoul IV, Ernesti JS, Butkevich EV, Duden R (2017) Drebrins and connexins: a biomedical perspective. Adv Exp Med Biol 1006:225–247. https://doi.org/10.1007/978-4-431-56550-5_13
66. Ye B, Shen H, Zhang J, Zhu YG, Ransom BR, Chen XC, Ye ZC (2015) Dual pathways mediate β-amyloid stimulated glutathione release from astrocytes. Glia 63(12):2208–2219. https://doi.org/10.1002/glia.22886
67. Liu L, Li CJ, Lu Y, Zong XG, Luo C, Sun J, Guo LJ (2015) Baclofen mediates neuroprotection on hippocampal CA1 pyramidal cells through the regulation of autophagy under chronic cerebral hypoperfusion. Sci Rep 5:14474. https://doi.org/10.1038/srep14474
68. Bejarano E, Yuste A, Patel B, Stout RF Jr, Spray DC, Cuervo AM (2014) Connexins modulate autophagosome biogenesis. Nat Cell Biol 16(5):401–414. https://doi.org/10.1038/ncb2934
69. Shibuya Y, Niu Z, Bryleva EY, Harris BT, Murphy SR, Kheirollah A, Bowen ZD, Chang CCY et al (2015) Acyl-coenzyme A:cholesterol acyltransferase 1 blockage enhances autophagy in the neurons of triple transgenic Alzheimer's disease mouse and reduces human P301L-tau content at the presymptomatic stage. Neurobiol Aging 36(7):2248–2259. https://doi.org/10.1016/j.neurobiolaging.2015.04.002
70. Li X, Song J, Dong R (2019) Cubeben induces autophagy via PI3K-AKT-mTOR pathway to protect primary neurons against amyloid beta in Alzheimer's disease. Cytotechnology 71(3):679–686. https://doi.org/10.1007/s10616-019-00313-6
71. Li Q, Liu Y, Sun M (2017) Autophagy and Alzheimer's disease. Cell Mol Neurobiol 37(3):377–388. https://doi.org/10.1007/s10571-016-0386-8